The geodynamo as a bistable oscillator

P. Hoyng [a,*], M.A.J.H. Ossendrijver [b] and D. Schmitt [c]

[a] SRON Laboratorium voor Ruimteonderzoek, Sorbonnelaan 2, 3584 CA Utrecht, The Netherlands;
[b] Kiepenheuer Institut für Sonnenphysik, Freiburg, Germany;
[c] Universitäts-Sternwarte, Göttingen, Germany

March 5, 2001

To appear in G.A.F.D.

Abstract

Our intent is to provide a simple and quantitative understanding of the variability of the axial dipole component of the geomagnetic field on both short and long time scales. To this end we study the statistical properties of a prototype nonlinear mean field model. An azimuthal average is employed, so that (1) we address only the axisymmetric component of the field, and (2) the dynamo parameters have a random component that fluctuates on the (fast) eddy turnover time scale. Numerical solutions with a rapidly fluctuating α reproduce several features of the geomagnetic field: (1) a variable, dominantly dipolar field with additional fine structure due to excited overtones, and sudden reversals during which the field becomes almost quadrupolar, (2) aborted reversals and excursions, (3) intervals between reversals having a Poisson distribution. These properties are robust, and appear regardless of the type of nonlinearity and the model parameters. A technique is presented for analysing the statistical properties of dynamo models of this type. The Fokker-Planck equation for the amplitude a of the fundamental dipole mode shows that a behaves as the position of a heavily damped particle in a bistable potential $\propto (1-a^2)^2$, subject to random forcing. The dipole amplitude oscillates near the bottom of one well and makes occasional jumps to the other. These *reversals* are induced solely by the overtones. Theoretical expressions are derived for the statistical distribution of the dipole amplitude, the variance of the dipole amplitude between reversals, and the mean reversal rate. The model explains why the reversal rate increases with increasing secular variation, as observed. Moreover, the present reversal rate of the geodynamo, once per $(2-3)\times 10^5$ year, is shown to imply a secular variation of the axial dipole moment of $\sim 15\%$ (about the current value). The theoretical dipole amplitude distribution agrees well with the Sint-800 data.

Keywords: geodynamo; reversals; secular variation; dynamo theory; helicity fluctuations; stochastic processes; bistable oscillator.

1 Introduction

It is known on paleomagnetic evidence that the Earth has had a magnetic field for at least 3.5×10^9 yr. There are indications that the field has always been largely dipolar. The dipole axis is aligned with the rotation axis to within $\lesssim 10^\circ$. Otherwise, intensity

*Corresponding author; e-mail: p.hoyng@sron.nl

and direction of the field vary on all time scales of a few 100 years and longer. The most spectacular aspect of the variability are the sudden polarity reversals. During a reversal the intensity of the dipole component becomes small and the dipole axis may make a few rapid swings. The dipole then grows in the opposite direction, and in $\lesssim 10$ kyr the whole process is completed and the field has reversed its direction. The process may also be interrupted and the dipole component may rebound to its original polarity state. This is called an aborted reversal or a magnetic excursion. The mean period between subsequent reversals is presently about $(2-3)\times 10^5$ yr. These and other properties of the geomagnetic field have been documented in great detail by Jacobs (1994) and Merrill *et al.* (1996).

The field is generally believed to originate from dynamo action in the liquid outer core of the Earth. Several groups have reported 3D hydromagnetic simulations of the geodynamo, demonstrating that self-sustained dynamo action is able to overcome the resistive decay of the currents in the outer core (Glatzmaier and Roberts, 1995a,b, 1996; Kageyama and Sato, 1997; Kuang and Bloxham, 1997; Olson *et al.*, 1999). The solid inner core plays a stabilising role and prevents the field from reversing too frequently (Hollerbach and Jones, 1993). In the 2.5D simulation of Sarson and Jones (1999) the stabilisation is achieved through a convection-driven meridional circulation, and fluctuations in the latter cause reversals. The simulations of Glatzmaier *et al.* (1999) demonstrate that frequency and polar paths of reversals depend strongly on the assumed radial heat flux pattern at the core-mantle boundary.

The idea that some kind of rapid variability may induce reversals has a long history, and the fact that the distribution of the intervals between successive reversals is Poissonian (Jacobs, 1994; Merrill *et al.*, 1996) also points in this direction. Parker (1969) and Levy (1972), and later Olson (1983), Olson and Hagee (1990), Le Mouël *et al.* (1997) and Narteau *et al.* (2000) have proposed that fluctuations in the helicity distribution of the convection may cause a reversal (see also Gibbons, 1998). These models were all based on the mean field concept.

The aim of this paper is to extend these mean field models just mentioned in two new directions. In the first place we present a theoretical framework with which the statistical properties of mean-field dynamos of the geo-type can be analysed, and we illustrate this technique by applying it to a specific model. In the second place we shall compare the theoretical predictions of our model in detail with the observed properties of the geomagnetic field.

In the mean field approximation the evolution of the large scale field $\langle \boldsymbol{B} \rangle$ is given by (Moffatt, 1978; Krause and Rädler, 1980):

$$\frac{\partial \langle \boldsymbol{B} \rangle}{\partial t} = \boldsymbol{\nabla} \times [\boldsymbol{v} \times + \alpha - (\beta + \eta)\boldsymbol{\nabla} \times] \langle \boldsymbol{B} \rangle \, . \tag{1}$$

The fluid motion $\boldsymbol{v} + \boldsymbol{u}$ consists of the mean flow $\boldsymbol{v}$, on which the turbulent convection $\boldsymbol{u}$ is superposed. The quantity η is the molecular resistivity, and β the turbulent resistivity. The parameters α and β are determined by the mean properties of the turbulent convection:

$$\alpha \simeq -\tfrac{1}{3}\langle \boldsymbol{u} \cdot \nabla \times \boldsymbol{u} \rangle \tau_{\rm c} \; ; \qquad \beta \simeq \tfrac{1}{3}\langle |\boldsymbol{u}|^2 \rangle \tau_{\rm c} \, . \tag{2}$$

The convection has a correlation time $\tau_{\rm c}$ (= eddy turnover time), and a correlation length $\lambda_{\rm c}$ (= eddy size). The validity of the mean field approach requires that the eddy Reynolds number $u\lambda_{\rm c}/\eta$ be much larger than 1, or that $\eta \ll \beta$ since $u\tau_{\rm c} \sim \lambda_{\rm c}$. Here we simply assume that we may ignore η with respect to β in (1). The mean helicity $\langle \boldsymbol{u} \cdot \nabla \times \boldsymbol{u} \rangle$ is nonzero in a rotating convecting medium, such as the fluid outer core of the Earth and the solar convection zone. The combined action of advection and shear (term $\propto \boldsymbol{v}\times$), diffusion

(term $\propto \eta + \beta$) and the α-effect is able to sustain a mean field $\langle \boldsymbol{B} \rangle$ (Moffatt, 1978; Krause and Rädler, 1980; Soward, 1991; Stix, 1991; Hoyng, 1992; Roberts and Soward, 1992).

Since we compare our model eventually to observations of the geomagnetic field, we indirectly apply the mean field concept to the geodynamo. This requires further discussion, which we postpone to Section 5.2.3 as we arrive to this topic. At this point the term "mean-field model of the geo-type" which we coined above just means an $\alpha\Omega$ model with a non-periodic fundamental mode of the dipole type. We focus on an $\alpha\Omega$ model because there are now strong indications that the inner core rotates $\lesssim 1^\circ$ yr^{-1} faster than the outer core (Song and Richards, 1996; Su *et al.*, 1996; Vidale *et al.*, 2000; Richards, 2000; for a different opinion see Souriau *et al.*, 1997; Laske and Masters, 1999). A similar effect has been observed in the hydromagnetic simulations (Glatzmaier and Roberts, 1996).

The average $\langle \cdot \rangle$ may be interpreted as an ensemble average or, as we shall do here, as an azimuthal average (Braginskii, 1965a,b). The latter may be regarded as an average over an incomplete ensemble, comprising only the system itself and all azimuthally rotated states. The fluctuations in our equations emerge as a natural consequence of the azimuthal average. There is only a finite number of convecting elements on a circle over which the average is taken, and these elements are renewed after each correlation time τ_c. Hence parameters like α, β defined in (2) and also the mean flow $\boldsymbol{v}$ must have a fluctuating component on the fast time scale τ_c. Fluctuations in α are probably the most important because $\boldsymbol{u} \cdot \nabla \times \boldsymbol{u}$ may have either sign, contrary to $|\boldsymbol{u}|^2$ (Otmianowska-Mazur *et al.*, 1997). Such fluctuations in α have been shown to explain the observed correlation between phase and amplitude of the solar dynamo (Ossendrijver *et al.*, 1996; Hoyng, 1993, 1996).

Schmitt *et al.* (2000) have recently applied these ideas in the context of the geodynamo. Their simulations reproduced important features of the geomagnetic field, and a theoretical analysis delivered (1) the amplitude distribution of the dipole component, (2) a simple physical picture of the reversal mechanism, and (3) a relation between the secular variation of the geomagnetic field and the mean time between reversals that agrees with the observations. Here we present a detailed numerical and theoretical study of this model that we define in Section 2. Numerical results are presented in Section 3, and an analysis of the statistical properties of the model follows in Section 4. A comparison of the theoretical predictions and the observed properties of the geodynamo is given in Section 5, and we discuss our results in Section 6.

2 Dynamo model

2.1 The linear system

We consider a simple axisymmetric dynamo in a spherical shell representing the outer core of the Earth, very similar to the one studied by Schmitt and Schüssler (1989). We do so because this model is adequate for our purpose, but as will become clear later, our method allows us to handle more complex models without much extra difficulty. The mean field $\langle \boldsymbol{B} \rangle$ is written as

$$\langle \boldsymbol{B} \rangle = \nabla \times A\,\boldsymbol{e}_\varphi + B\,\boldsymbol{e}_\varphi \;, \tag{3}$$

which splits $\langle \boldsymbol{B} \rangle$ into its poloidal part $\perp \boldsymbol{e}_\varphi$ and toroidal part $\parallel \boldsymbol{e}_\varphi$, the unit vector in the azimuthal direction (we employ spherical polar co-ordinates r, θ, ϕ). As a further simplification we make a local approximation to a radial spherical wave:

$$A = \frac{\alpha_0 R^2}{\beta}\, P(\theta,t)\, \frac{\cos kr}{kr} \quad ; \qquad B = T(\theta,t)\, \frac{\cos kr}{kr} \;. \tag{4}$$

This allows a crude modeling of the effect of radial turbulent diffusion. The factor $\alpha_0 R^2/\beta$ ensures that P and T have the same dimension. The dynamo parameter β is considered to be a constant, and the constants α_0 and R are reference values of α and the radial position. The mean flow $\boldsymbol{v}$ in the outer core is written as $\boldsymbol{v} = \boldsymbol{\Omega} \times \boldsymbol{r} = \Omega r \sin\theta\, \boldsymbol{e}_\varphi$. Ansatz (3) and (4) are substituted in the dynamo equation (1) and we make the $\alpha\Omega$-approximation to obtain (Ossendrijver *et al.*, 1996):

$$\frac{\partial \boldsymbol{b}}{\partial \tau} = G\boldsymbol{b}\,, \quad \text{with} \quad \boldsymbol{b}(\theta,\tau) = \begin{pmatrix} P \\ T \end{pmatrix}\,, \tag{5}$$

and

$$G = \begin{pmatrix} L & \alpha/\alpha_0 \\ C\frac{\partial}{\partial\theta}\sin\theta & L \end{pmatrix}\,. \tag{6}$$

The dimensionless time τ is measured in units of τ_d. The dynamo number C, the diffusion time τ_d, and the diffusion operator L are given by:

$$C = \alpha_0 R^4 \Omega'/\beta^2\,, \qquad \tau = t/\tau_\mathrm{d}\,, \qquad \tau_\mathrm{d} = R^2/\beta\,, \tag{7}$$

$$L = \frac{1}{\sin\theta}\frac{\partial}{\partial\theta}\sin\theta\frac{\partial}{\partial\theta} - \frac{1}{\sin^2\theta} - (kR)^2\,. \tag{8}$$

Here $\mathrm{d}\Omega/\mathrm{d}r \equiv \Omega'$ is the differential rotation which we take to be constant. The radial co-ordinate r has become a free parameter and has been set equal to the radial reference position R. The boundary conditions are $P = T = 0$ at $\theta = 0,\, \pi$. We adopt the customary choice that $\alpha \propto \cos\theta$ (Moffatt, 1978; Soward, 1991; Schmitt and Schüssler, 1989):

$$\alpha/\alpha_0 = \cos\theta\,. \tag{9}$$

Here α_0 is the value of α at the North pole. Later, when we consider nonlinear effects, relation (9) will contain a function of $\langle \boldsymbol{B} \rangle$ on the right hand side.

2.1.1 Eigenfunctions and parameters

The eigenfunctions $\boldsymbol{b}_i(\theta)$ and eigenvalues λ^i of G obey

$$G\boldsymbol{b}_i = \lambda^i \boldsymbol{b}_i\,; \qquad \boldsymbol{b}_i = \begin{pmatrix} P_i \\ T_i \end{pmatrix}\,. \tag{10}$$

The operator G is not self-adjoint, and the eigenvalues λ^i and eigenmodes $\boldsymbol{b}_i$ are in general complex. The eigenfunctions of the adjoint $\tilde{G}$ satisfy

$$\tilde{G}\tilde{\boldsymbol{b}}_i = \lambda^{i*}\tilde{\boldsymbol{b}}_i\,; \qquad \tilde{\boldsymbol{b}}_i = \begin{pmatrix} \tilde{P}_i \\ \tilde{T}_i \end{pmatrix}\,, \tag{11}$$

where * indicates complex conjugation. With proper normalisation $\{\boldsymbol{b}_i\}$ and $\{\tilde{\boldsymbol{b}}_i\}$ form a bi-orthonormal set

$$(\tilde{\boldsymbol{b}}_i, \boldsymbol{b}_j) = \delta_{ij} \tag{12}$$

with respect to the inner product

$$(\boldsymbol{b}_1, \boldsymbol{b}_2) = \int_0^\pi \mathrm{d}\theta \sin\theta\, (P_1^* P_2 + T_1^* T_2)\,. \tag{13}$$

Table 1. First eigenvalues and eigenmode types of G for $kR = 0.5$ and $\alpha/\alpha_0 = \cos\theta$.

i	Parity of $T(\theta)$ [a]	$C = C_0 = 57.9$		$C = C_\mathrm{m} = 100$	
		$\Re\lambda^i$ [b]	$\Im\lambda^i$ [c]	$\Re\lambda^i$ [b]	$\Im\lambda^i$ [c]
0	a	0	0	0.527	0
1	s	−2.76	4.41	−2.16	5.88
2	a	−8.67	4.97	−8.21	6.04
3	s	−15.9	6.13	−15.7	7.70

[a] s = symmetric, a = antisymmetric with respect to the equator $\theta = \pi/2$; $P(\theta)$ and $T(\theta)$ have opposite symmetry, $P(\theta)$ and $\tilde{P}(\theta)$ the same symmetry, as do $T(\theta)$ and $\tilde{T}(\theta)$.
[b] The eigenvalue problem being parabolic, the growth rate $\Re\lambda^i$ is a decreasing series, asymptotically $\sim i(i+1)$.
[c] All overtones are periodic, $\Im\lambda^i \neq 0$ for $i \geq 0$.

Details on the normal and adjoint eigenvalue problem may be found in Kleeorin and Ruzmaikin (1984), Ossendrijver (1996) and Ossendrijver *et al.* (1996). An arbitrary field $\boldsymbol{b}(\theta,\tau)$ may be expanded into eigenfunctions:

$$\boldsymbol{b}(\theta,\tau) = \sum_k a_k(\tau)\boldsymbol{b}_k(\theta) \ , \tag{14}$$

with

$$a_i = (\tilde{\boldsymbol{b}}_i, \boldsymbol{b}) \ . \tag{15}$$

This relation follows from (14) by using the bi-orthonormality property.

The behavior of the eigenvalues as a function of C is quite complicated (Schmitt and Schüssler, 1989). The requirement that the fundamental mode be a non-periodic dipole restricts the values of the parameters to $0 < kR < 1$ and $C > 0$. For given kR there is a critical dynamo number C_0 below which all eigenmodes are damped. We need to be a little more precise in our notation, and associate henceforth with C_0 the reference value α_0. The dynamo number at which the model operates is denoted as C_m, with which we associate the reference value α_m:

$$C_0 \equiv \alpha_0 R^4\Omega'/\beta^2 \ , \qquad C_\mathrm{m} \equiv \alpha_\mathrm{m} R^4\Omega'/\beta^2 \ . \tag{16}$$

The model has three free parameters, kR, C_m and one associated with the strength of the fluctuations to be introduced later. In our simulations we take $kR = 0.5$, and then $C_0 = 57.9$, while $1/k = 2R$ measures the radial length scale of the field. Furthermore we adopt $C_\mathrm{m} = 100$. More details are given in Table 1 and in Sections 5.2.3 and 5.2.4.

2.2 Nonlinear feedback and fluctuations

2.2.1 Nonlinearity

The model operates at $C_\mathrm{m} > C_0$ and is supercritical, featuring an exponentially growing field. Nonlinearities will prevent unlimited growth, but their role in the dynamo equation (1) is poorly understood and simple models are frequently used in want of better. An example is α-quenching, which in its simplest form amounts to replacing α_m in $\alpha = \alpha_\mathrm{m}\cos\theta$ by $\alpha_\mathrm{m}(1 - \mathrm{const}\cdot\langle\boldsymbol{B}\rangle^2)$ (Rüdiger, 1973). The idea is that an increasing magnetic field reduces the helicity of the flow, and thereby α_m. In order to keep the theoretical

analysis manageable we shall adopt a simplified model (Brandenburg *et al.*, 1989), and replace *local* quenching by a *global* one: $\alpha_{\rm m} \to \alpha_{\rm m}(1 - {\rm const} \cdot \int \langle \boldsymbol{B} \rangle^2 \, {\rm d}^3 r)$:

$$\alpha = \alpha_{\rm m}(1-q)\cos\theta \,, \tag{17}$$

$$q \simeq {\rm const}' \int_0^\pi (\Re T)^2 \sin\theta \, {\rm d}\theta \tag{18}$$

$$\simeq {\rm const}''(\Re a_0)^2 \,. \tag{19}$$

In the second line we have used that the toroidal part of $\langle \boldsymbol{B} \rangle$ is much stronger than the poloidal part in the $\alpha\Omega$ approximation, and $\Re$ is added because the fields are in general complex, but the quenching is done by the real field. Due to the fluctuations in α (to be introduced below) overtones will be excited besides the fundamental mode, and in the third line we keep only the contribution of the fundamental mode (expansion coefficient a_0), as that is usually the dominant mode.

2.2.2 Nonlinear equilibrium

The operator G in (6) has now $h(q)\cos\theta$ as its upper right element, and $C = C_{\rm m}$ in its lower left element. The quenching function $1 - q$ is written temporarily as $h(q)$. Since global quenching leaves the angular dependence of α intact, the dynamo possesses a unique nonlinear equilibrium, independent of the shape of $h(q)$. The evolution of $\boldsymbol{b}$ is governed by an effective $\boldsymbol{b}$-dependent dynamo number $C_{\rm m}h(q)$, and the nonlinear equilibrium must coincide with the solution of the linear equation at the critical dynamo number C_0. The equilibrium is stable if $dh/dq < 0$, and the equilibrium value of q is determined by $C_{\rm m}h(q_0) = C_0$, or $\alpha_{\rm m}h(q_0) = \alpha_0$. This shows that the constants in (18) and (19) are irrelevant, and that changing their value merely changes the unit in which $\langle \boldsymbol{B} \rangle$ is measured. It turns out to matter very little what we choose for q in numerical simulations, as long as it is a quadratic measure of the field strength. We shall adopt (17) and (19) because a simple functional form of $h(q)$ and q is an asset in the theoretical analysis.

2.2.3 Fluctuations

As argued in Section 1, $\boldsymbol{v}$, α and β will exhibit rapid residual variability on the time scale $\tau_{\rm c}$ of the turbulent flow. Following earlier work on the solar dynamo (Hoyng, 1993; Ossendrijver *et al.*, 1996) we focus on fluctuations in α, as these are expected to be the most important, and (17) changes into:

$$\alpha = \alpha_{\rm m}(1-q)\cos\theta + \delta\alpha(\theta,\tau) \,, \tag{20}$$

$$\delta\alpha = \alpha_0 \frac{f F(\theta,\tau)}{\sqrt{2N_{\rm c}\sin\theta}} \,. \tag{21}$$

We reiterate that the fluctuations $\delta\alpha$ in (20) are not added ad hoc. They are a necessary consequence of the azimuthal average, but since little is known about their strength and spatial distribution we resort to a model. Helicity fluctuations with a correlation length ('cell size') $\lambda_{\rm c}$ and correlation time $\tau_{\rm c}$ are assumed to be homogeneously distributed in the outer core, so that $\delta\alpha$, being an azimuthal average, is proportional to $N^{-1/2}$, where $N = 2N_{\rm c}\sin\theta$ is the number of cells on a circle of constant latitude. The total number of cells on a sphere is $4N_{\rm c}^2/\pi$. F is a random function of θ for given τ, and of τ for given θ, with zero mean and unit variance. In numerical experiments, F is updated once every correlation time, independently in every latitude interval $\theta_{\rm c} = \pi/N_{\rm c}$. The parameter f

measures the unknown relative strength of the fluctuations. In the nonlinear equilibrium, when $\alpha_{\rm m}(1-q_0)=\alpha_0$, each cell has a mean contribution $\alpha_0\cos\theta$ to α, while the superposed fluctuations have an r.m.s. magnitude of $f\alpha_0$ per cell. In the simulations reported here we do not allow for magnetic quenching of the fluctuations, and Section 3.3 explains why.

Our stochastic turbulence model is much simpler than the hierarchical model of Narteau *et al.* (2000) but it is adequate for our purposes. In fact most details of the model like cell size and distribution are irrelevant. The only thing that matters is that the mean part of α scales as $\cos\theta$ (which is standard) and the fluctuating part as $(\sin\theta)^{-1/2}$, i.e. increasing towards the poles. There is no problem near the poles as the field becomes zero there. In our simulations we use $\tau_{\rm c}=0.05$ and $N_{\rm c}=10$, see further Section 5.2.4. It will be shown later that all statistical properties depend only on the combination $f^2\tau_{\rm c}/N_{\rm c}^2$. This is the third parameter of the model.

2.3 Model equations

Eqs. (5) and (6) with (20) for α define our geodynamo model. It is useful to express the value of q in equilibrium, q_0, in terms of a new supercriticality parameter s:

$$s \equiv \frac{C_{\rm m}}{C_0} - 1 = \frac{q_0}{1-q_0}\,, \tag{22}$$

since $C_{\rm m}(1-q_0)=C_0$. For $kR=0.5$ and $C_{\rm m}=100$ we have $s=0.728$ and $q_0=0.421$. Next, q from (19) is written as

$$q = q_0(\Re a_0)^2\,, \tag{23}$$

where a_0 is now measured in units of its value in nonlinear equilibrium. Since the amplitude $\Re a_0$ of the fundamental mode occurs so frequently, we introduce

$$a \equiv \Re a_0\,. \tag{24}$$

After some rearranging relation (20) becomes

$$\frac{\alpha}{\alpha_0} = \cos\theta + s(1-a^2)\cos\theta + \frac{\delta\alpha}{\alpha_0}\,. \tag{25}$$

In the numerical and theoretical analysis the field $\boldsymbol{b}$ will be expanded in eigenfunctions belonging to C_0. This is an expansion around the nonlinear equilibrium and therefore rather efficient. In conformity with (25), Eq. (5) for $\boldsymbol{b}$ is now replaced by

$$\frac{\partial \boldsymbol{b}}{\partial \tau} = \Big[G + s(1-a^2)E + V\Big]\boldsymbol{b}\,, \tag{26}$$

where G pertains to the critical dynamo number C_0, and $a=\Re\,(\tilde{\boldsymbol{b}}_0,\boldsymbol{b})$ according to (15), where $\tilde{\boldsymbol{b}}_0$ is the adjoint of the fundamental mode belonging to C_0. Furthermore

$$E=\begin{pmatrix}0 & \cos\theta\\ 0 & 0\end{pmatrix}\;;\qquad V=\begin{pmatrix}0 & \delta\alpha/\alpha_0\\ 0 & 0\end{pmatrix}\,. \tag{27}$$

The first term on the r.h.s. of (26) describes the linear evolution, the second term the nonlinearity and, for small a, the supercriticality, while the third represents the effect of the fluctuations. Since the nonlinearity does not depend on the sign of the field there are two nonlinear equilibria, $a=1$ and $a=-1$. This feature reflects the fact that the MHD equations are invariant under the transformation $\boldsymbol{B}\;\rightarrow\;-\boldsymbol{B}$.

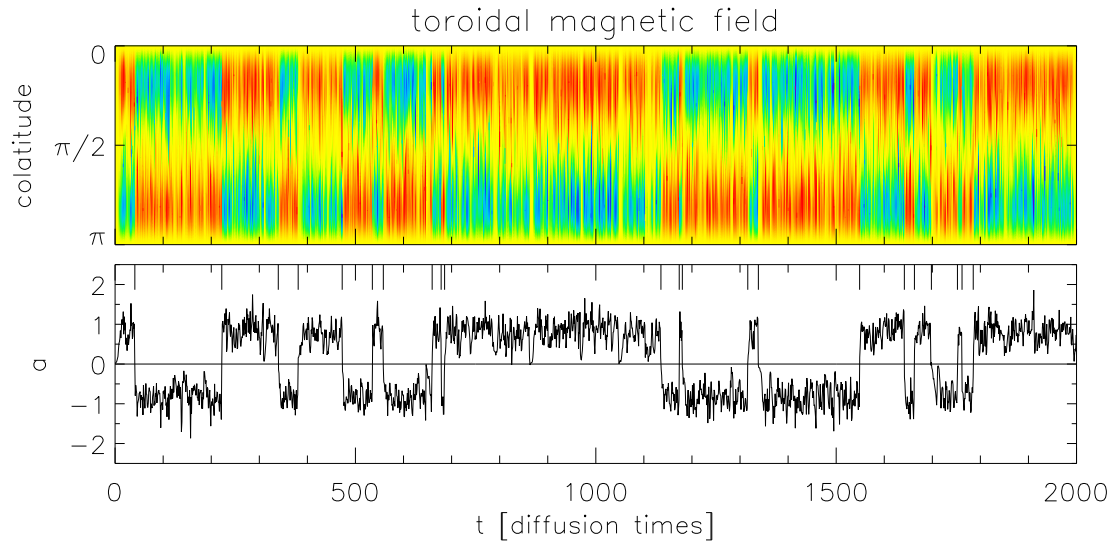

Figure 1: Numerical solution of Eq. (26) for our standard case with forcing parameter $f = 6.4$. Shown is a colour plot of the toroidal field $\Re T$, together with the normalised amplitude $a = \Re a_0$ of the fundamental dipole mode. The spacing of the printed data is 100 time steps, suppressing any variability at shorter time scales. Transient excitation of the overtones produces a fine structure with the appearance of vertical stripes. Vertical bars mark the position of a reversal. Aborted reversals are not well visible due to the reduced time resolution; they occur e.g. at $\tau = 825$, 863, 1048, but also at $\tau = 1475$; the event at $\tau = 648$ is an excursion.

3 Simulations

3.1 Standard case

Numerical solution of Eq. (26) is straightforward. The model is relatively simple and simulations extending over $\sim 10^5$ turbulent diffusion times τ_d or more are quite feasible. Figures 1 and 2 show our standard case.[1] It shares several characteristic features with the geomagnetic record (Jacobs, 1994; Merrill *et al.*, 1996):

(1). A dominantly dipolar field of rapidly varying amplitude, on which a fine structure is superposed due to transient excitation of the overtones. The dipole mode amplitude a fluctuates around its nonlinear equilibrium value.

(2). Occasional sudden polarity reversals. The forcing parameter f has been tuned so that the mean time between reversals is about $100\,\tau_\mathrm{d}$ (from a long run).

(3). Aborted reversals, where a changes sign for a short moment, after which the field returns to its previous polarity state, and magnetic excursions.

The agreement with the geomagnetic data is discussed in detail in Section 5.2. Note that our definition[2] of (aborted) reversals and excursions is dictated by theoretical convenience rather than by geophysical practice. The parity of the field displayed in Figure 2 is defined as (Brandenburg *et al.*, 1989):

$$\mathcal{P} = \frac{\mathcal{E}_S - \mathcal{E}_A}{\mathcal{E}_S + \mathcal{E}_A}\,, \tag{28}$$

where $\mathcal{E}_{S,A} = \int_0^\pi (\Re T_{S,A})^2 \sin\theta \, \mathrm{d}\theta$ is a measure of the energy in the symmetric, antisymmet-

[1] The simulations shown in all figures have been generated on a 60 point equidistant θ-grid on $[0, \pi]$, time step $\Delta\tau = 10^{-2}$, $kR = 0.5$, $C_\mathrm{m} = 100$, $\tau_\mathrm{c} = 5 \times 10^{-2}$ and $N_\mathrm{c} = 10$.

[2] We define a reversal as an odd number of zero crossings of a within a few diffusion times τ_d. An aborted reversal refers to an even number of zero crossings in rapid succession. In an excursion a 'approaches zero' but does not change sign. This definition is subjective, but there is no obvious alternative. There remain ambiguities, e.g. three 'closely spaced' zero crossings may also be an aborted event followed by a reversal.

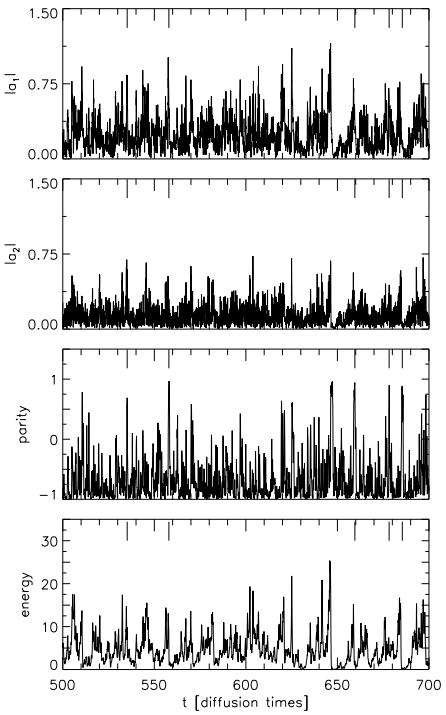

Figure 2: The section between $\tau = 500$ and $\tau = 700$ from Figure 1 at higher resolution (spacing 5 time steps). From top to bottom: normalised magnitude of the complex overtone amplitude $|a_1|$ and $|a_2|$, both computed from (15), the parity $\mathcal{P}$ of the field and the 'energy' $\int_0^\pi (\Re T)^2 \sin\theta \, \mathrm{d}\theta$. Vertical bars mark the position of a reversal.

ric component of the toroidal field ($T_S(\theta) = T(\theta) + T(\pi - \theta)$; $T_A(\theta) = T(\theta) - T(\pi - \theta)$). Except during (aborted) reversals and excursions, the field is largely antisymmetric ($\mathcal{P} \simeq -1$), and therefore dipolar as the fundamental dipole mode is much stronger than the antisymmetric overtones.

3.2 Reversals and aborted reversals

Figures 3 and 4 show the evolution of the toroidal field during an (aborted) reversal in detail. From inspection of a number of these events the following picture emerges:

(1). During an (aborted) reversal the field has a tendency to become symmetric ($\mathcal{P} \uparrow +1$ in Figure 2) because the overtones dominate, and frequently mode # 1 (a quadrupole) stands out. A quasi-periodic behavior is sometimes observed with a period of the order of τ_d. This is due to the fact that all overtones are periodic. For example, if mode # 1 dominates, the period would be about $2\pi/5.88 \simeq 1.1$ diffusion times, from Table 1.

(2). The onset of a reversal is characterised by a decrease in $|a|$, combined with a sudden enhancement ($\lesssim 0.5\,\tau_\mathrm{d}$) of the amplitude of mode # 1 and/or 2, or rather of the magnitude of the toroidal field T_+ of the overtones, defined in (38). However, the realisation of $\delta\alpha(\theta, \tau)$ must be 'favorable', as not all jumps in T_+ and/or the mode coefficients produce a reversal, see Figure 2.

(3). Just after the zero crossing during an (aborted) reversal, the whole field $\boldsymbol{b}$ often ends up being small, i.e. all expansion coefficients are small. In that case the field enters into a recovery phase to the nonlinear equilibrium. This happens because when $|a| \ll 1$ the nonlinearity is switched off and then (26) says, very roughly, that $\boldsymbol{b}$ grows exponentially.

(4). Although there are fast events lasting $\sim 0.5\,\tau_\mathrm{d}$, the typical duration of a reversal is $\sim 3\tau_\mathrm{d}$. The observed duration of a reversal is $\lesssim 10$ kyr (Merrill *et al.*, 1996), and it would follow that $\tau_\mathrm{d} \sim 3$ kyr. The mean time between reversals is then $100\,\tau_\mathrm{d} \sim 3 \times 10^5$

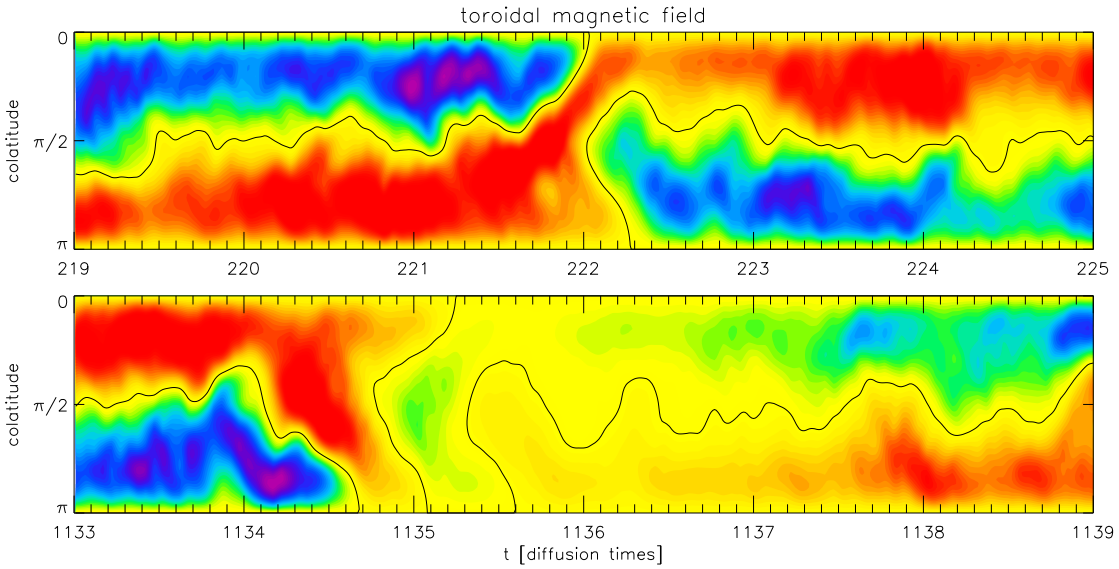

Figure 3: Two reversals of Figure 1 at full resolution. The black line indicates where the toroidal field is zero. The top panel shows a very fast event. In the bottom panel the field becomes quasi-periodic. This is due to the first overtone, a quadrupole, with a period of 1.1 (see text). The recovery phase after $\tau = 1135$ is roughly an exponential growth with a time scale of the order of Λ^{-1}, see (34). The grey scale in this and the next figure has a steep gradient near zero, to enhance the contrast between the two polarities.

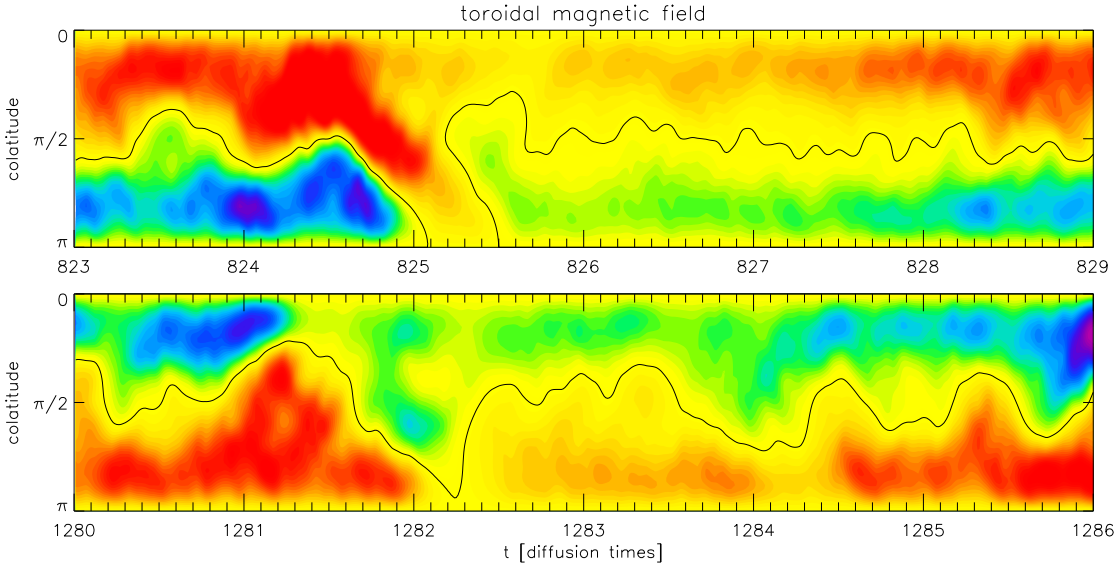

Figure 4: An aborted reversal (top) and an excursion at $\tau \simeq 1282$ (bottom), both from Figure 1. The black line indicates where the toroidal field is zero. Aborted reversals and excursions are formally different in that the dipole mode does or does not change sign, but have often a similar appearance.

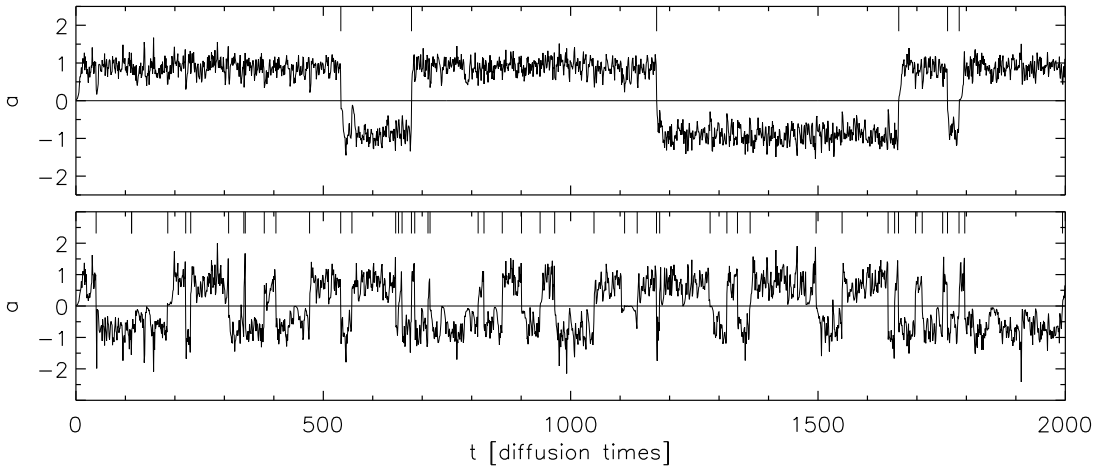

Figure 5: Amplitude a of the fundamental dipole mode for $f = 5.4$ (top) and $f = 7.4$ (bottom). The case $f = 6.4$ is shown in Figure 1. The other parameters are as in Figure 1, and in all three cases the same random series has been used. Vertical bars mark the position of reversals.

yr, which is about the observed value of the geodynamo in recent times.

3.3 Other cases and scaling

Figure 5 shows a for two different values of the forcing parameter f. It is evident that the reversal rate is extremely sensitive to the strength of the forcing. We have verified that the dominant scaling of mean properties (such as the mean time between reversals and the r.m.s. variability between reversals) with the strength of the forcing is through the combination $f^2\tau_c/N_c^2$. We demonstrate later that the reversal rate depends exponentially on $f^2\tau_c/N_c^2$.

We have tried other types of nonlinearity, such as (1) α as in (17) and q from (18), (2) $\alpha = \alpha_m \cos\theta/(1+q)$ and q from (19), and (3) local instead of global quenching, cf. Section 2.2.1. We have also investigated the effect of changing C_m and kR, and we have allowed for magnetic quenching of the fluctuations $\delta\alpha$. The conclusion from all these tests is that the statistical properties of the dipole mode are not materially affected. For example, we found that magnetic quenching of the fluctuations reduces the mean reversal rate and the r.m.s. variability between reversals of the dipole amplitude, because the effective strength f of the forcing diminishes. However, the quenching may be offset by increasing the free parameter f. Such a simulation has very similar statistical properties as a run with a smaller f and no quenching. Similar observations hold when we change the model parameters or the type of nonlinearity. For that reason there is no magnetic quenching of the fluctuations in the simulations reported here, and we concentrate our efforts on the standard case defined by Eq. (26).

4 Statistical analysis

Let us recapitulate where we stand. We employ a well-known equation (1) for the axisymmetric component of the magnetic field, and add fluctuations in the dynamo parameter α as a new element. These fluctuations must be present on general grounds, and they are seen in the hydromagnetic simulations, but their impact has never been analysed in the context of the geodynamo. Apart from the model parameters C_m and kR, the only free parameter is f, or rather $f^2\tau_c/N_c^2$. This defines the physics in our model, which is

by all means simple. The multiplicative noise term excites all eigenmodes of (1). The fundamental mode has a rapidly varying amplitude and occasional random reversals, and we shall show in Sections 5.2 and 6 that it reproduces the behavior of the geomagnetic dipole field on short as well as long time scales.

It is straightforward to infer the statistical properties of the model from simulations of the type presented above. The advantage of a simple model is that these properties may also be determined theoretically, by applying techniques from the theory of stochastic processes. This is the second new element of our work. It requires a considerable amount of analysis, but the reward is a clear insight in the physics of the model. The dipole amplitude turns out to behave as a randomly forced particle in a bistable potential, and the mean reversal rate is given by the equivalent of the Kramers escape rate of a thermally activated strongly damped particle. The technique that we introduce below does not rely on the details of the model. It is assumed that the fundamental mode is non-periodic, but otherwise our analysis can be readily applied to more complicated dynamo models.

4.1 Coupled mode equations

The starting point is the equation for the mode amplitudes a_i, which follows by taking $d/d\tau$ of (15) and using (26) and (14):

$$\frac{\mathrm{d}a_i}{\mathrm{d}\tau} = \lambda^i a_i + s(1-a^2)E_{ik}a_k + V_{ik}a_k \ , \tag{29}$$

with $a = \Re a_0$. In these coupled mode equations all a_k are in units of the value of a_0 in nonlinear equilibrium. We adopt henceforth the summation convention for double lower indices as in $E_{ik}a_k$ and $V_{ik}a_k$, but *not* in $\lambda^i a_i$. The matrix elements are defined as

$$E_{ik} = (\tilde{\boldsymbol{b}}_i, E\boldsymbol{b}_k) = \int_0^\pi \mathrm{d}\theta \, \sin\theta\cos\theta \, \tilde{P}_i^* T_k \ , \tag{30}$$

$$V_{ik}(\tau) = (\tilde{\boldsymbol{b}}_i, V\boldsymbol{b}_k) = \int_0^\pi \mathrm{d}\theta \, \sin\theta \, (\delta\alpha/\alpha_0) \, \tilde{P}_i^* T_k \ . \tag{31}$$

A special role will be played by $E_{00} = \int_0^\pi \mathrm{d}\theta \, \sin\theta \, \cos\theta \, \tilde{P}_0 T_0 = 1.048$. The first term on the right hand side in (29) describes the linear evolution, and the λ^i are the eigenvalues at $C = C_0$ listed in Table 1. The second term is due to the supercriticality and the nonlinearity that drive the system to the nonlinear equilibrium ($a_0 = \pm 1$; $a_i = 0$, $i \geq 1$). The third term is a multiplicative noise term, representing the perturbations by the fluctuations.

4.2 Fokker-Planck Equation

The behavior of the mode amplitudes is illustrated in Figure 6. The proper tool for analysing the statistical properties of the fundamental mode is the probability distribution $p(a,\tau)$ of its amplitude $a = \Re a_0$, which obeys the following Fokker-Planck equation:

$$\frac{\partial p}{\partial \tau} = -\frac{\partial}{\partial a} Sp + \frac{1}{2}\frac{\partial^2}{\partial a^2} Dp \ . \tag{32}$$

The derivation of this equation is rather complex and relegated to Appendices A and B. Here we simply summarize the result of these computations, and much of the physical interpretation follows later. The Fokker-Planck equation describes how the probability density p evolves under the influence of systematic effects (drift coefficient S) and random effects (diffusion coefficient D), see Risken (1984), Gardiner (1990) or Van Kampen (1992). The drift coefficient S is given by

$$S = \mu(1-a^2)a + g_1(a) \simeq \Lambda(1-a^2)a \ , \tag{33}$$

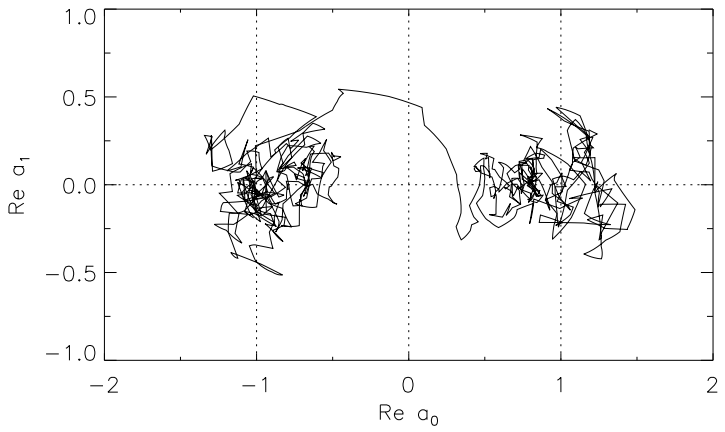

Figure 6: The overtone amplitude $\Re a_1$ is plotted against the amplitude of the fundamental mode $a = \Re a_0$ for $f = 5.4$ (taken from the run shown in Figure 5, top, near $\tau = 680$). The amplitude of the overtone fluctuates rapidly, while the fundamental mode is tied to the equilibrium positions $a = \pm 1$, making occasional jumps from one side to the other.

with

$$\mu \equiv sE_{00} = 0.763 \,, \qquad \Lambda \equiv \lambda^0|_{C=C_{\rm m}} = 0.527 \tag{34}$$

The second expression in (33) is an approximation for small a which is adequate for our purposes. Details may be found in Appendix B.1. The diffusion coefficient D is equal to (see Appendix B.2):

$$D = D_0 a^2 + D_1(a) \,, \tag{35}$$

$$D_0 = \frac{\pi f^2 \tau_{\rm c}}{2N_{\rm c}^2} \int_0^\pi {\rm d}\theta \, \sin\theta \, (\tilde{P}_0 T_0)^2 \,, \tag{36}$$

$$D_1 = \frac{\pi f^2 \tau_{\rm c}}{2N_{\rm c}^2} \int_0^\pi {\rm d}\theta \, \sin\theta \, \tilde{P}_0^2 \, \langle T_+^2 \rangle|_a \,. \tag{37}$$

The integral $\int_0^\pi {\rm d}\theta \, \sin\theta \, (\tilde{P}_0 T_0)^2$ in (36) equals 3.529. The symbol T_+ is defined as the toroidal field of the overtones,

$$T_+ = \Re \sum_{k \geq 1} a_k T_k = \Re(T - a_0 T_0) \,. \tag{38}$$

The fluctuations have a direct effect on a through the term $V_{00} a_0$ in (29). The corresponding diffusion coefficient is $D_0 a^2$. There is also an indirect effect (the term $V_{0k} a_k$, $k \geq 1$) that produces a fluctuating contribution to a through stochastic forcing of overtones, represented by $D_1(a)$. For later use we expand D to order a^2:

$$D \simeq \Delta_0 a^2 + \Delta_1 \,, \tag{39}$$

with

$$\Delta_0 = D_0 + \tfrac{1}{2} D_1''(0) \,; \qquad \Delta_1 = D_1(0) \,. \tag{40}$$

Here we have used that $D_1'(0) = 0$ since it is clear from (37) that $D_1(-a) = D_1(a)$. The approximations in (33) and (39) will be justified in Section 5.1.

4.3 Particle-in-well analogy

Readers not familiar with stochastic methods should retain just one thing from the previous section: the fluctuations $\delta\alpha$ render the dipole amplitude a a stochastic variable

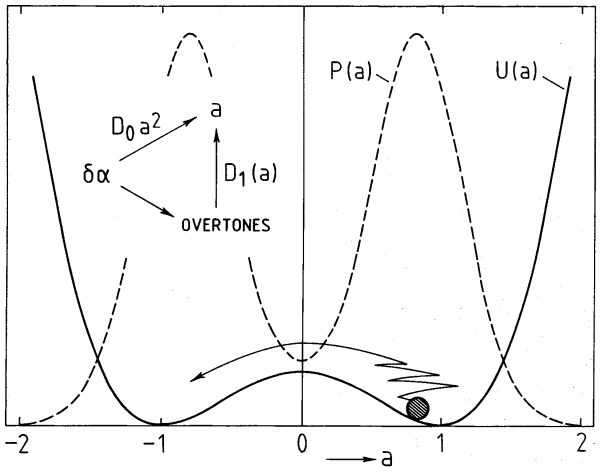

Figure 7: The amplitude of the fundamental dipole mode behaves as the position of a heavily damped particle subject to random forcing, in a bistable potential $U(a) = \frac{1}{4}\Lambda(1-a^2)^2$. As shown in the text, the fluctuations act directly on a (diffusion coefficient $D_0 a^2$), but this causes no reversals, and through the overtones (diffusion coefficient $D_1(a)$). The effect of the overtones is not restricted to a small region near $a = 0$. For the standard run D_1 is larger than $D_0 a^2$ for $|a| \lesssim 1$ (Section 5.1). The dashed curve is the stationary amplitude distribution $p(a)$ from (43) for $\gamma = 3$ and $c^2 = 0.2$.

with a probability distribution p evolving according to a kind of diffusion equation (32). This should be intuitively clear by itself, regardless of any mathematical detail. The only remarkable thing is that the diffusion coefficient D depends on the total non-dipole toroidal field, see (35) – (37). This means that all dependence on individual overtones has disappeared from (32), although we set out from eq. (29) in terms of individual mode amplitudes. Appendix E explains how this comes about.

The Fokker-Planck equation (32) admits a simple interpretation, since it also determines the probability distribution of the position a of a heavily damped, randomly forced particle in a bistable potential U given by $-\partial U/\partial a = S$:

$$U \simeq \tfrac{1}{4}\Lambda(1-a^2)^2 \,. \tag{41}$$

This particle-in-well paradigm will be used extensively below. The particle (i.e. the dipole amplitude) resides in one of the wells and performs a random motion near the bottom at $a = \pm 1$ due to fluctuations, with occasional jumps to the other side, see Figure 7. These correspond to the irregular magnetic field variations during intervals of one polarity and to a reversal, respectively. The geodynamo is thus pictured as a bistable oscillator. The central hill of U at $a = 0$ is due to the supercriticality, and the walls beyond $a = \pm 1$ are due to the nonlinearity. The fluctuations $\delta\alpha$ determine the variability of the dynamo. It is straightforward to obtain the stationary solution of (32):

$$p(a) \;\propto\; \frac{1}{D}\exp\left(\int_0^a \frac{2S}{D}\,\mathrm{d}a'\right) \tag{42}$$

$$\propto\; \left(1+\frac{a^2}{c^2}\right)^{\gamma c^2+\gamma-1} \exp(-\gamma a^2)\,. \tag{43}$$

This is the theoretical distribution of the amplitude a of the dipole mode. The parameters γ and c^2 and are defined as dimensionless measures of $U(0)$ and $D(0)$, respectively:

$$\gamma = \Lambda/\Delta_0 \;; \qquad c^2 = \Delta_1/\Delta_0 \,. \tag{44}$$

They determine $p(a)$ and therefore many statistical properties of the dipole amplitude. The combination of a steeply rising power-law and a sharply decreasing exponential makes that $p(a)$ has two peaks near $a = \pm 1$ where most of the probability is concentrated, see Figure 7. We shall show in Section 5.2 that the observed dipole amplitude distribution follows the theoretical expression (43) rather well.

We note that $c^2 \approx D_1(0)/D_0$, or in view of (36) and (37):

$$c^2 \propto \left(\frac{\text{r.m.s. toroidal field at a reversal}}{\text{r.m.s. toroidal field between reversals}} \right)^2 . \tag{45}$$

Hence c^2 may also be interpreted as a dimensionless measure of the r.m.s. toroidal field at a reversal. The scaling of c^2 and γ with the model parameters is discussed in Appendix E.

4.4 The reversal mechanism

It is straightforward to show that reversals must be fast events, caused by interaction with the overtones. The argument consists of three steps:

(1). If there are no overtones then (29) reduces to ($a_k = 0$ for $k \geq 1$; $\lambda^0 = 0$):

$$\frac{\mathrm{d}a_0}{\mathrm{d}\tau} = s(1 - a^2)E_{00}a_0 + V_{00}(\tau)a_0 . \tag{46}$$

The noise term is multiplicative, and the noise amplitude becomes arbitrarily small for small a_0. This prevents reversals, as can be seen by rewriting (46) in terms of $a = \Re a_0$, using that E_{00} and V_{00} are real:

$$\frac{\mathrm{d}\,\ln a}{\mathrm{d}\tau} = s(1 - a^2)E_{00} + V_{00}(\tau) , \tag{47}$$

i.e. $\ln a$ performs a restricted random walk and a cannot change sign: no reversals.

(2). For most of the time the dipole amplitude a resides near one of the minima of $U(a)$ at $a = \pm 1$. Now consider what happens if a goes *rapidly* to zero, through a series of favorable fluctuations. The overtones, although damped, do not follow suit immediately. According to (29) the evolution of a is then governed by these overtones:

$$\frac{\mathrm{d}a}{\mathrm{d}\tau} = \Re \sum_{k \geq 1} (sE_{0k} + V_{0k})a_k . \tag{48}$$

Hence a is temporarily driven by *additive* noise, and if the realisation of the fluctuations is right, a reversal may ensue.

(3). We may now conclude that a reversal cannot be a slow event, because if the evolution toward a reversal is slow, the overtones have the opportunity to decay. The system then enters into the state described by Eq. (47) and the result is an excursion. The flip becomes a flop, so to speak.

Let's rephrase the argument from the point of view of the Fokker-Planck equation. We begin with a dipole amplitude $a = 1$, i.e. we consider Eq. (32) with initial condition $p(a, 0) = \delta(a - 1)$. For $\tau > 0$ the probability distribution $p(a, \tau)$ broadens and a quasi-equilibrium distribution is quickly established in the well at $a = 1$, on a time scale Λ^{-1}. On a much longer time scale, the probability starts to creep diffusively over the hill at $a = 0$ (i.e. reversals set in) and the well at $a = -1$ gets slowly filled in, leading to the final distribution (43). Writing (32) as $\partial p/\partial \tau = -\partial F/\partial a$, then $F = Sp - \frac{1}{2}\partial(Dp)/\partial a$ is

the probability current. Since S and $\mathrm{d}D/\mathrm{d}a$ vanish at $a = 0$, the probability current at $a = 0$ is, according to (35), equal to:

$$F \;=\; \tfrac{1}{2}D(0)\,\frac{\partial p}{\partial a}\bigg|_{a=0} \;=\; \tfrac{1}{2}D_1(0)\,\frac{\partial p}{\partial a}\bigg|_{a=0}\,, \tag{49}$$

There is no contribution from $D_0 a^2$. Reversals are caused by a small but finite diffusion coefficient $D_1(0)$ solely due to the overtones, cf. (37) and (38): $D_1(0)$ is determined by $\langle T_+^2\rangle|_{a=0}$, the mean square non-dipole toroidal field during reversals. Since this does not favor any overtone, it also follows that it will, in the long run, be impossible to attribute a reversal to any overtone in particular.

4.5 The statistics of field reversals

A variety of statistical properties of a may be inferred from (43), and here we consider three that are directly linked to observable features. For analytical work a 'parabolic approximation' to $p(a)$ is often useful (Van Kampen, 1992), valid for sufficiently large γ:

$$p(a) \;\propto\; \exp[\psi(a)] \;\simeq\; \exp\left[\psi_{\mathrm{m}} + \tfrac{1}{2}\psi''_{\mathrm{m}}(a - a_{\mathrm{m}})^2\right]\,, \tag{50}$$

with

$$\psi(a) \;=\; -\gamma a^2 + (\gamma c^2 + \gamma - 1)\ln(1 + a^2/c^2)\,, \tag{51}$$

from which we infer that

$$a_{\mathrm{m}} \;=\; \pm\left(1 - \frac{1}{\gamma}\right)^{1/2}\,, \tag{52}$$

$$\psi_{\mathrm{m}} \;=\; 1 - \gamma + (\gamma c^2 + \gamma - 1)\ln\left(\frac{\gamma c^2 + \gamma - 1}{\gamma c^2}\right)\,, \tag{53}$$

$$\psi''_{\mathrm{m}} \;=\; -\,\frac{4\gamma(\gamma - 1)}{\gamma c^2 + \gamma - 1}\,. \tag{54}$$

The value of γ is restricted to $\gamma > 1$, otherwise $p(a)$ consists of a single peak at $a = 0$.

4.5.1 Variability of the field between reversals

The average amplitude $\langle a\rangle$ between reversals follows by integrating over a single peak of $p(a)$:

$$\langle a\rangle \;=\; \frac{\int_{-\infty}^{\infty} a p(a)\,\mathrm{d}a}{\int_{-\infty}^{\infty} p(a)\,\mathrm{d}a} \;\simeq\; a_{\mathrm{m}} \;=\; \left(1 - \frac{1}{\gamma}\right)^{1/2}\,. \tag{55}$$

where $p(a)$ is taken from (50), assuming that the field (the particle) resides in the well at $a = 1$. The mean value of a is smaller than 1. In Figures 1 and 5, a fluctuates asymmetrically around $+1$ or -1, so that the mean of $|a|$ between reversals is indeed smaller than 1. The physical origin is the asymmetry of the well around $|a| = 1$ in Figure 7, and the fact that $D(a)$ increases with a. The amplitude stays longer in the region $|a| < 1$ because the random motion is slower there than in $|a| > 1$.

In a similar manner we may compute the variance around the mean. The result may be written as:

$$\frac{\langle (a - \langle a\rangle)^2\rangle}{\langle a\rangle^2} \;\simeq\; \frac{\gamma c^2 + \gamma - 1}{4(\gamma - 1)^2}\,. \tag{56}$$

This is independent of the units in which a is expressed, and may thus be directly connected to the measured relative variability of the dipole field between reversals.

4.5.2 Mean reversal rate

A classic problem in the theory of stochastic processes is the mean escape time of a stochastically driven particle from an interval $[a_1, a_2]$. Presently we may relate the mean reversal time to the mean escape time $\langle T_\mathrm{e}\rangle$ of the particle from the region $0 \le a < \infty$, starting from an initial position $a' > 0$, which according to standard theory is equal to (Gardiner, 1990; Van Kampen, 1992):

$$\langle T_\mathrm{e}\rangle \;=\; 2\int_0^{a'} \frac{\mathrm{d}y}{D(y)p(y)} \int_y^\infty p(z)\,\mathrm{d}z\;. \tag{57}$$

This expression is almost independent of the initial position a' as long as it is near the bottom of the well ($a' \approx 1$). As the particle escapes from $[0, \infty]$ it is located at the top of U at $a = 0$. It may then make one or more additional rapid zero crossings, but irrespective of that, one would think it has a chance of $\frac{1}{2}$ to fall in the well at $a = -1$, and of $\frac{1}{2}$ to fall back to $a = 1$ where it came from. According to our terminology[2] the former event is a reversal, the latter an aborted reversal. It would follow that the mean waiting time for a reversal is $2\langle T_\mathrm{e}\rangle$, and this is then also the mean time $\langle T_\mathrm{r}\rangle$ *between* successive reversals (see Van Kampen, 1992, exercise on p. 47). But the two probabilities are not equal, and $\langle T_\mathrm{r}\rangle$ is only approximately equal to $2\langle T_\mathrm{e}\rangle$, see Appendix F, where we show that:

$$\langle T_\mathrm{r}\rangle \approx 2\langle T_\mathrm{e}\rangle \;\simeq\; \frac{\pi}{\Lambda}\left(\frac{2}{c^2}\right)^{1/2}\left(\frac{\gamma c^2+\gamma-1}{\gamma-1}\right)^{1/2}\exp(\psi_\mathrm{m}) \tag{58}$$

$$\sim\; \frac{\pi\sqrt{2}}{\Lambda}\left(\frac{c^2}{1+c^2}\right)^{1/2}\exp(K\gamma)\;, \tag{59}$$

with

$$K \;=\; -1+(1+c^2)\ln\left(\frac{1+c^2}{c^2}\right)\;. \tag{60}$$

Relation (59) is an asymptotic expansion of (58) for large γ. It shows that $\langle T_\mathrm{r}\rangle$ scales approximately as $\exp[\mathrm{const}\cdot U(0)/(f^2\tau_\mathrm{c}/N_\mathrm{c}^2)]$, see Appendix E, which explains the very strong dependence on f. There is a close analogy with the escape rate of a strongly damped *thermal* particle from a potential well, a problem first considered by Kramers in 1940 (Van Kampen, 1992). A thermal particle has an energy $\sim kT$ (k = Boltzmann's constant, T = temperature), but must acquire an energy $U(0) - U(1) = U(0)$ to be able to escape to the other well in Figure 7. The chance for this to happen (i.e. the inverse mean escape time) is $\propto \exp[-U(0)/kT]$. The parameter $f^2\tau_\mathrm{c}/N_\mathrm{c}^2$ thus serves as a kind of effective temperature. We demonstrate in Section 5 that relation (56) and (58) agree well with our simulations and with the observed properties of the geomagnetic dipole moment.

4.5.3 Distribution of polarity intervals

According to standard theory (Risken, 1984; Gardiner, 1990; Van Kampen, 1992) the distribution of the lengths T_r of polarity intervals between successive reversals can be proven to be Poissonian, $\propto \exp(-T_\mathrm{r}/\langle T_\mathrm{r}\rangle)$ for $T_\mathrm{r} \gg \Lambda^{-1}$, and from a number of long runs we have verified this Poissonian character. We shall not enter into any details, as this result is intuitively evident, given the stochastic nature of the model and the short memory of the fluctuations.

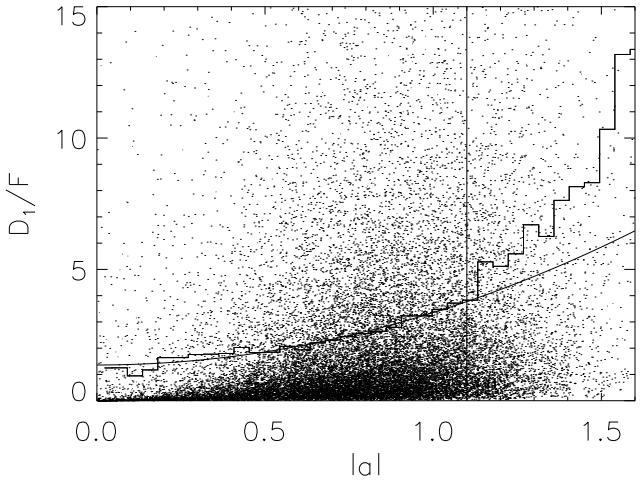

Figure 8: The dots, 5×10^4 in total, are the numerically computed values of D_1/F ($F = \pi f^2 \tau_c / 2N_c^2$) for the standard case, as explained in the text. The histogram is constructed by determining the average in the corresponding bin. The continuous curve ($1.36 + 2.00a^2$) is the result of a least-square-fit of a quadratic function to the histogram levels, weighted by the number of points in the bin, for $a \leq 1.1$. For larger a the contribution of a^4 becomes appreciable.

5 Model validation

We wish to raise two issues here. The first is how reliable are the analytical results derived in the previous section, and the second how do the properties of the model compare to those of the geodynamo.

5.1 Internal consistency

In order to verify the results of the previous sections, we must be able to express c^2 and γ in terms of the model parameters, but this is unfortunately not yet possible, cf. Appendix E. As next best option we have determined D_1 numerically from a long run, as follows. During the simulations T_+ is known at all times, which permits computing a value of D_1 at the current value of a with the help of (37) – omitting the averaging there. We do so with a spacing of 1 diffusion time to ensure statistically independent draws, and the result is plotted in Figure 8. The data are then fitted to a quadratic function of a. For the standard case the result is

$$D_1 \simeq \frac{\pi f^2 \tau_c}{2N_c^2} (1.36 + 2.00a^2) , \tag{61}$$

or, upon adding $D_0 a^2$:

$$D \simeq \frac{\pi f^2 \tau_c}{2N_c^2} (1.36 + 5.52a^2) , \tag{62}$$

from which Δ_0 and Δ_1 follow. Since $\pi f^2 \tau_c / 2N_c^2 = 3.22 \times 10^{-2}$, we obtain

$$c^2 \simeq 0.246 ; \qquad \gamma \simeq 2.96 . \tag{63}$$

It follows from (56) and (58) that $\langle (a - \langle a \rangle)^2 \rangle / \langle a \rangle^2 \simeq 0.17$ and $\langle T_r \rangle \simeq 94$. The simulation had 468 reversals in 5×10^4 diffusion times, whence $\langle T_r \rangle = 107 \pm 5$, while $\langle (a - \langle a \rangle)^2 \rangle / \langle a \rangle^2$

Table 2. Comparison of numerical and analytic results.

run [a]	f	c^2	γ	$\frac{\langle (a-\langle a\rangle)^2\rangle}{\langle a\rangle^2}$		$\langle T_\mathrm{r}\rangle$	
#				(56)	from run	(58)	from run
1	4.4	0.318	9.04	0.04	0.03	12000	10700 ± 5300
2	5.4	0.299	5.15	0.08	0.07	480	519 ± 53
3	6.4	0.246	2.96	0.17	0.16	94	107 ± 5
4	7.4	0.240	1.82	0.47	0.30	35	37.6 ± 1
5 [b]	8.4	0.228	1.09	1.0	0.50	35	18.7 ± 0.4

[a] All runs have $N_\mathrm{c} = 10$, $\tau_\mathrm{c} = 5 \times 10^{-2}$, and comprise 5×10^4 diffusion times. Run # 3 is the standard case.
[b] Run # 5 is outside the validity range of the asympotic analysis of Section 4.5 because γ is so close to 1.

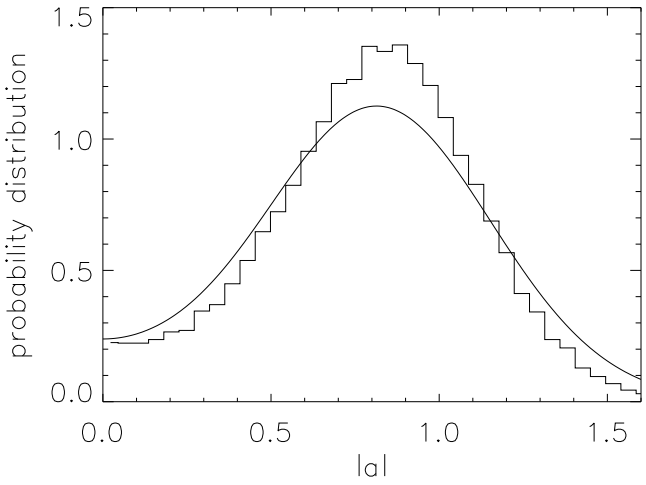

Figure 9: Numerically determined amplitude distribution $p(a)$, constructed by binning subsequent values of a during the simulation, and the theoretical distribution (43) (drawn curve). Both curves have been normalised to unit area. The discrepancy is explained in the text.

was measured to be 0.16. These results are summarised in Table 2, together with those of a few more simulations for different values of the forcing parameter f. The agreement between the values predicted by (56) and (58), and the values measured from the simulations is satisfactory, certainly in view of the fact that (58) holds only approximately.

Figure 9 compares the numerically determined amplitude distribution $p(a)$ with the theoretical result (43). Here the agreement seems less good. The origin of the discrepancy lies in the approximate expression (33) for S. We have computed $g_1(a)$ numerically, in the same way as we did for D_1, and found that expression (33) is correct for $|a| \lesssim 0.4$, but for larger $|a|$ deviations occur. In view of the dependence of (42) on S deviations in $p(a)$ should be expected. The discrepancy virtually disappears if we use a more accurate expression for S by evaluating the next term in $g_1(a)$ as indicated in Appendix B.1 (Hoyng *et al.*, 2001). This correction can be shown to have little effect on the mean reversal time $\langle T_\mathrm{r}\rangle$.

5.2 Comparison with the geodynamo

The observed properties of geomagnetic field reversals may be summarised as follows (Jacobs, 1994; Merrill *et al.*, 1996). The mean time $\langle T_{\rm r}\rangle$ between successive polarity reversals has decreased over the last 160 Myr, and is now $(2-3)\times 10^5$ yr. A reversal takes $\lesssim 10$ kyr. There is no correlation between the lengths of subsequent polarity intervals, nor between polarity and length of polarity intervals. The distribution of the interval lengths $T_{\rm r}$ between reversals is well described by a nonstationary Poisson process (because the mean reversal rate is changing).

These features are all reproduced by our model, where a typical reversal lasts $3\tau_{\rm d}$ and $\langle T_{\rm r}\rangle$ is about 100 diffusion times for $f = 6.4$ It follows that $\tau_{\rm d} \sim 3$ kyr and $\langle T_{\rm r}\rangle \sim 3\times 10^5$ yr. And the statistics of the reversals is, by construction, independent of the field direction. A reversal is necessarily a fast event in our model. The quasi-periodic behavior that we sometimes observe during a reversal due to the temporary dominance of periodic overtones may be related to the rapid variability the geomagnetic field is sometimes reported to have during a reversal (Coe *et al.*, 1995).

5.2.1 Secular variation and mean reversal rate

Our model cannot predict the mean reversal rate of the geodynamo as the effective forcing parameter $f^2\tau_{\rm c}/N_{\rm c}^2$ is free. However, it does predict the correct relation between the variance of the dipole amplitude between reversals (the secular variation of the dipole mode, in geophysical parlance) and the mean reversal rate. From the particle-in-well analogy it is obvious that such a relation must exist. As the particle is subjected to larger random perturbations it will oscillate in the well with larger amplitude, but it will also jump more frequently from one side to the other, as is evident from Table 2 and Figure 5. Such a trend between secular variation and mean reversal rate is indeed suggested in the geomagnetic record (McFadden and Merrill, 1995), and in hydromagnetic simulations (Glatzmaier *et al.*, 1999). We thus offer a very simple theoretical explanation for this phenomenon.

The agreement is more than qualitative, as the numbers work out quite well. The current mean reversal rate of once per ~ 100 diffusion times, implies $\langle(a-\langle a\rangle)^2\rangle/\langle a\rangle^2 \simeq 0.16$, cf. Table 2. In order to compare this with the geodynamo we have determined the relative variance of the dipole component from three Virtual Axial Dipole Moment (VADM) records: (1) the last 130 kyr (Figure 4.9 of Merrill *et al.* (1996)), (2) between 2 and 2.5 Myr ago in the Matuyama chron and (3) between 2.5 and 3 Myr ago in the Gauss chron, both from Valet and Meynadier (1993). We may take a to be proportional to the ordinate in the figures, because the amplitude of the poloidal *dipole* field, which determines the VADM, is proportional to a. The result is that $\langle(a-\langle a\rangle)^2\rangle/\langle a\rangle^2$ equals 0.1, 0.15 and 0.2, respectively, in reasonable agreement with the prediction of our model.

5.2.2 The Sint-800 data

After completion of the simulations reported here, detailed VADM measurements have become available (Guyodo and Valet, 1999). These data allowed us to construct the observed dipole amplitude distribution. A preliminary comparison with the theoretical distribution $p(a)$ of (43) is shown in Figure 10. The parameters correspond closely to run #2 (Table 2), except that $c^2 = 0.25$ instead of 0.3. The agreement is surprisingly good in view of the fact that we have made no attempt to improve the fit by changing the model parameters kR and $C_{\rm m}$. A parameter study is now in progress, and the results will be reported elsewhere (Hoyng *et al.*, 2001). We anticipate that a modest change of

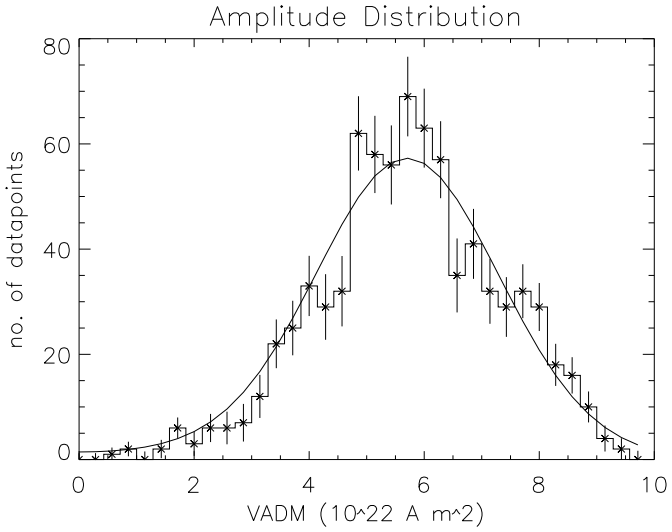

Figure 10: The Sint-800 data is a 800 kyr record of the Virtual Axial Dipole Moment (VADM) of the geomagnetic field comprising 800 data points with a spacing of 1000 yr (Guyodo and Valet, 1999). The histogram is the amplitude distribution of these data sampled in 35 bins. The drawn curve is a fit to the theoretical amplitude distribution $p(a)$ from (43) for $\gamma = 5.15$ and $c^2 = 0.25$. The χ^2 of the fit corresponds to 1σ. A fit to the parameters of run #2 ($\gamma = 5.15$ and $c^2 = 0.3$) has a χ^2 of 2σ. Data for $t > 780$ kyr (the time of the last reversal) are treated as positive because of the $p(-a) = p(a)$ symmetry.

the parameters will suffice to bring our model into agreement with the data. It appears therefore that over the past 800 kyr the geodynamo behaved rather closely conform run #2. The mean reversal time $\langle T_r \rangle \sim 500\tau_d \sim 1.5$ Myr of that run would be consistent with the fact that the last reversal took place 780 kyr ago, but this requires more careful statistics.

5.2.3 Mean field approximation

Last but not least, we discuss the applicability of the mean field approximation with which all our results have been obtained. From $\tau_d = R^2/\beta \sim 3$ kyr and $R \sim 3500$ km we infer $\beta \sim 10^6$ cm^2 s^{-1}. Since the conductivity of the core is 6×10^5 S m^{-1} (Merrill *et al.*, 1996, p. 274) the resistivity is $\eta \sim 1.3 \times 10^4$ cm^2 s^{-1}. Hence the eddy magnetic Reynolds number would be $\beta/\eta \sim 80$. We conclude that application of mean field theory seems reasonable, although estimates of this kind may always be stretched one way or the other.

To verify the consistency of the $\alpha\Omega$ approximation we consider the Reynolds numbers $C_\alpha = \alpha_m R/\beta$ and $C_\Omega = R^3\Omega'/\beta$. A value for Ω' follows from claims that the inner core rotates $\lesssim 1^\circ$ yr^{-1} faster than the outer core (references quoted in Section 1). This suggests that there is a negative gradient $\Omega' \sim -1^\circ$ yr$^{-1}/\Delta R$. Taking $\Delta R = 2300$ km (difference of outer and inner core radii) and $R = 3500$ km we obtain $C_\Omega \sim -100$ and $C_\alpha \sim -1$, since $C_m = C_\alpha C_\Omega$. Hence $|C_\alpha| \ll |C_\Omega|$. We are not claiming to prove that mean field theory and the $\alpha\Omega$ approximation actually hold in the geodynamo, but merely that their application here is self-consistent.

5.2.4 Characteristic numbers

The $\alpha\Omega$ approximation would in fact apply for any C_m larger than $C_0 = 57.9$, and $C_m = 100$ is chosen for two reasons. (1) It leads to a reasonable time scale for oscillations around

the nonlinear equilibrium of $(2\Lambda)^{-1} \simeq 1$ diffusion time or about 3 kyr. The fine structure of vertical spikes in Fig. 1, due to variable excitation of the first few overtones, would thus have a typical time scale of $(\Re\lambda)^{-1} \lesssim 1$ kyr, according to Table 1. This is in fair agreement with the geomagnetic data (Merrill *et al.*, 1996). (2). It follows that $\alpha_{\rm m} \sim -3 \times 10^{-3}$ cm s^{-1}. This is a reasonable value in the sense that $|\alpha|$ is everywhere smaller than the typical convective speed $u \sim 10^{-2}$ cm s^{-1} in the outer core.[3]

The specific values of $\tau_{\rm c}$, $\lambda_{\rm c}$ and $N_{\rm c}$ are not very important as only $f^2\tau_{\rm c}/N_{\rm c}^2$ matters. But an eddy turnover time of $\tau_{\rm c} = 0.05$ corresponds to 150 yr and implies an eddy size of $\lambda_{\rm c} \sim u\tau_{\rm c} \sim 500$ km. And $N_{\rm c} = 10$ would mean 20 convective cells on a great circle, or $4N_{\rm c}^2/\pi \sim 130$ on a sphere. The fluctuations in α are large. In the nonlinear equilibrium the ratio of the fluctuating and the systematic term in (20) is $\delta\alpha_{\rm r.m.s.}/\alpha_0 \cos\theta = (\alpha_0 f/\sqrt{2N_{\rm c}\sin\theta})/\alpha_0 \cos\theta \gtrsim 2.5$ for the standard run.

6 Discussion and summary

We have presented a technique to analyse the statistical properties of the axisymmetric component of the geomagnetic field in the mean field approximation. Key elements are (1) nonlinear restriction of the magnitude of the field, and linear supercritical operation for small fields, (2) a non-periodic fundamental dipole mode and periodic overtones, (3) fluctuations in the dynamo parameter α. Application to a geodynamo model shows a variable, dominantly dipolar magnetic field, with sudden reversals during which the field tends to be quadrupolar. These features are generic, and appear irrespective of the type of nonlinearity and the model parameters, which allowed us to work with a simple nonlinearity (global α-quenching). The amplitude of the fundamental mode turns out to behave as the position of a stochastically driven particle in a bistable potential. This simple physical picture provides a conceptual framework for understanding the variability of the axial dipole component of the geomagnetic field on short as well as long time scales. Our main results are

(1). A theoretical prediction for the amplitude distribution of the dipole mode that is confirmed by the observed distribution (the Sint-800 record).

(2). A relation between the secular variation of the dipole mode and the mean reversal rate. The current mean time between reversals of $(2-3) \times 10^5$ yr was shown to imply the observed relative variability of the axial dipole moment of about 15%. More generally, the model predicts that during epochs of smaller secular variability the reversal rate is also smaller, and the available observations indicate that this is actually the case (McFadden and Merrill, 1995).

(3). Reversals are sudden events, lasting $\lesssim 10$ kyr, during which the field structure becomes almost symmetric (quadrupolar). Sometimes a rapid variability is visible during a reversal with a period of the order of a diffusion time ($\sim$ 3 kyr), due to the periodic overtones.

Our work is a generalisation of that of Parker (1969), and is also related to the interacting-dipoles model of Mazaud and Laj (1989) and the multiple-scale turbulence model of Narteau *et al.* (2000). Instead of the reaction of the dynamo to a single jump in α as Parker did, the effect of a stationary level of fluctuations in α is studied over long times. The model permitted a detailed theoretical analysis and long simulations (here up to $\sim$ 150 Myr), both far beyond what 3D hydromagnetic simulations can afford. Other statistical features not considered here, for example the autocorrelation function of the

[3]The maximum possible value of $|\alpha|$ is the r.m.s. convective flow speed and is attained for maximally helical convection.

dipole amplitude, the relative frequency of excursions of a given magnitude, etc., may also be computed.

We stress that our results are not contingent on the simplicity of the dynamo model, as they depend only on the eigenvalues and certain overlap integrals of the eigenfunctions. In particular, they do not rely on our model being one-dimensional. Any model having a nonperiodic fundamental mode and periodic first overtones would exhibit qualitatively similar properties, and the technique developed here can be directly applied to these more complicated models. The most desirable generalisation would be a 2D model, with radial distance as an independent co-ordinate. That would permit us to allow for the effect of the inner core, and to verify, for example, the suggestion of Gubbins (1999) that the duration of a reversal is gauged by the resistive decay time of the inner core, since the field must penetrate the inner core for a full reversal.

The statistical properties of the dipole amplitude turned out to depend only on $\langle T_+^2 \rangle$, the mean square toroidal field of the overtones. For that reason we have refrained from analysing the cause of a reversal. Such a cause, e.g. a particularly strong overtone, may always be found in individual cases, but it will be impossible to discern a general pattern. In our model reversals can, in the mean, not be pinpointed to any overtone in particular. The situation is however not completely satisfactory because it remains unclear why we did not find reversals in a comparable study of an α^2 dynamo (Hoyng and Van Geffen, 1993). And our analysis is not complete as we have not been able to express $\langle T_+^2 \rangle|_{a=0}$ and hence the parameters c^2 and γ in terms of $f^2\tau_c/N_c^2$. Solution of this problem would enable us to bypass the elaborate fitting procedure of Section 5.1.

The origin of the fluctuations lies in the turbulent convection and the azimuthal average. This is an average over an incomplete ensemble, and therefore all averages (α, β, etc.) will have a random component, fluctuating on the correlation time scale τ_c (the eddy turnover time). 'Normal' ensemble averages are constant because the ensemble contains all possible states of the system. Motivated by our work on the phase-amplitude correlation in the solar dynamo (Ossendrijver *et al.*, 1996; Hoyng, 1993, 1996), we have concentrated on fluctuations in α. However, the effect of fluctuations in β and $\boldsymbol{v}$ has never been studied yet.

Technically, the fluctuations appear as multiplicative noise. Some authors have studied the effect of additive noise (Crossley *et al.*, 1986; Meinel and Brandenburg, 1990; Farrell and Ioannou, 1999a,b). While this is interesting in itself, care is needed to ascertain a physical basis for the extra term. For example, an additive noise term in the dynamo equation (1) renders it inhomogeneous, leading to the unphysical feature that the magnitude of the field would be fixed, even when nonlinearities are ignored.

Predictions of the magnitude of the fluctuations, the parameter f in our model, are not available, neither from theory nor from hydromagnetic simulations. A model of randomly renovating 'cells', homogeneously distributed in the outer core, has so far proven to be adequate. The required fluctuations are large. In the nonlinear equilibrium the ratio of the fluctuating and the systematic term in (20) is $\delta\alpha_{\rm r.m.s.}/\alpha_0 \gtrsim 2.5$ for the standard run. Roughly the same number is required to explain the observed phase-amplitude correlation in the solar cycle (Ossendrijver *et al.*, 1996), but this is probably a coincidence. Mean field dynamos are apparently very insensitive to rapid variations of α. But it remains unknown if such high fluctuation levels can actually be attained. This, together with the scaling of $\langle T_+^2 \rangle|_{a=0}$ with $f^2\tau_c/N_c^2$, are the two main unresolved issues.

The mean reversal rate is extremely sensitive to the forcing due to the exponential scaling with $f^2\tau_c/N_c^2$. If $f^2\tau_c/N_c^2$ changes by a factor 2 (f from 6.4 to 4.4 in Table 2) the mean time between reversals increases by a factor 100 to about 20 Myr. This might explain the long polarity bias in the Cretaceous, some 100 Myr ago (Jacobs, 1994; Merrill

et al., 1996). Our model illustrates that a relatively small change of the mean properties of the convection in the outer core may appear observationally as if the geodynamo switches to a different, non-reversing physical state, as suggested by McFadden and Merrill (1995), while in reality the reversal *mechanism* remains operative all the time, but the reversal *rate* becomes very small.

The slow increase of the reversal rate and the secular variation since the Cretaceous (Jacobs, 1994; Merrill *et al.*, 1996; McFadden and Merrill, 1995) could likewise be due to a slow increase of the parameter $f^2\tau_c/N_c^2$ by a factor 2. This idea has been elaborated by Schmitt *et al.* (2000). It is tempting to speculate that such a change in the parameters of the convection is related to the gradual evolution of the inner core with time, or to changes in the heat flux pattern at the core-mantle boundary (Glatzmaier *et al.*, 1999).

A final remark on the role of nonlinearities. The nonlinearity in our model restricts the dipole amplitude a to a finite range, while the supercriticality forces it away from zero. In this 'backbone structure', linear multiplicative noise causes the dipole amplitude to perform a random walk of restricted amplitude. During a reversal the model dynamo evolves as a linear system, since $1 - a^2 \simeq 1$ in (26) and (29). That may hold for the geodynamo as well, because the field decreases by a factor 4 or more, and the Lorentz force is then a factor $10 - 20$ smaller than normal, at least globally. Under those circumstances a linear evolution is not unreasonable. The fluctuations, however, are a manifestation of nonlinear turbulence, and the question whether nonlinear interactions or fluctuations cause variability and reversals is therefore semantic. They are ultimately caused by nonlinear effects. The point of our work is that on the fast timescale of the eddy-turnover time the effect of these nonlinearities is practically indistinguishable from that of a multiplicative noise term. For the longer timescales this is no longer true and nonlinearities remain essential. The added advantage is that many properties of the nonlinear system are now open to analytic evaluation, as we have shown. This is in fact a well-known and very successful approach in many areas of physics.

7 Acknowledgements

SRON is supported financially by NWO, the Netherlands Organisation for Scientific Research. M.A.J.H.O. acknowledges funding by the Deutsche Forschungsgemeinschaft. We are indebted to Prof. N.G. van Kampen for helpful discussions, and to Mr. J. Wiersma who suggested to us the compact proof of Appendix D.

8 References

Braginskii, S.I., 'Self-excitation of a magnetic field during the motion of a highly conducting fluid,' *Sov. Phys.–JETP 20*, 726-735 (1965a).

Braginskii, S.I., 'Theory of the hydromagnetic dynamo,' *Sov. Phys.–JETP 20*, 1462-1471 (1965b).

Brandenburg, A., Krause, F., Meinel, R., Moss, D. and Tuominen, I., 'The stability of nonlinear dynamos and the limited role of kinematic growth rates,' *Astron. Astrophys. 213*, 411-422 (1989).

Christensen, U., Olson, P. and Glatzmaier, G.A., 'A dynamo model interpretation of geomagnetic field structures,' *Geophys. Res. Lett. 25*, 1565-1568 (1998).

Coe, R.S., Prévot, M. and Camps, P., 'New evidence for extraordinarily rapid change of the geomagnetic field during a reversal,' *Nature 374*, 687-692 (1995).

Crossley, D., Jensen, O. and Jacobs, J., 'The stochastic excitation of reversals in simple dynamos,'

Phys. Earth Planet. Inter. 42, 143-153 (1986).

Farrell, B.F. and Ioannou, P.J., 'Optimal excitation of magnetic fields,' *Astrophys. J. 522*, 1079-1087 (1999a).

Farrell, B.F. and Ioannou, P.J., 'Stochastic dynamics of field generation in conducting fluids,' *Astrophys. J. 522*, 1088-1099 (1999b).

Gardiner, C.W., *Handbook of Stochastic Methods*, Springer-Verlag, Berlin (1990).

Gibbons, S.J., 'The Parker-Levy reversal mechanism,' *Phys. Earth Planet. Inter. 106*, 129-137 (1998).

Glatzmaier, G.A. and Roberts, P.H., 'A three-dimensional self-consistent computer simulation of a geomagnetic field reversal,' *Nature 377*, 203-209 (1995a).

Glatzmaier, G.A. and Roberts, P.H., 'A three-dimensional convective dynamo solution with rotating and finitely conducting inner core and mantle,' *Phys. Earth Planet. Inter. 91*, 63-75 (1995b).

Glatzmaier, G.A. and Roberts, P.H., 'Rotation and magnetism of the Earth's inner core,' *Science 274*, 1887-1891 (1996).

Glatzmaier, G.A., Coe, R.S., Hongre, L. and Roberts, P.H., 'The role of the Earth's mantle in controlling the frequency of geomagnetic reversals,' *Nature 401*, 885-890 (1999).

Gubbins, D., 'The distinction between geomagnetic excursions and reversals,' *Geophys. J. Int. 137*, F1-F3 (1999).

Guyodo, Y. and Valet, J.-P., 'Global changes in intensity of the Earth's magnetic field during the past 800 kyr,' *Nature 399*, 249-252 (1999).

Hollerbach, R. and Jones, C.A., 'Influence of the Earth's inner core on geomagnetic fluctuations and reversals,' *Nature 365*, 541-543 (1993).

Hoyng, P., 'Mean field dynamo theory,' in: *The Sun, A Laboratory for Astrophysics* (Eds. J.T. Schmelz and J.C. Brown), Kluwer Academic Publishers, Dordrecht, 99-138 (1992).

Hoyng, P., 'Helicity fluctuations in mean field theory: an explanation for the variability of the solar cycle?' *Astron. Astrophys. 272*, 321-339 (1993).

Hoyng, P., 'Is the solar cycle timed by a clock?' *Sol. Phys. 169*, 253-264 (1996).

Hoyng, P. and Van Geffen, J.H.G.M., 'Stochastic excitation of global magnetic fields by fluctuations in the mean helicity,' *Geophys. Astrophys. Fluid Dynamics 68*, 203-236 (1993).

Hoyng, P., Schmitt, D. and Ossendrijver, M.A.J.H., 'A theoretical analysis of the observed variability of the geomagnetic dipole field,' *Phys. Earth Planet. Inter.*, submitted (2001).

Jacobs, J.A., *Reversals of the Earth's Magnetic Field*, Cambridge University Press (1994).

Kageyama, A. and Sato, T., 'Generation mechanism of a dipole field by a magnetohydrodynamic dynamo,' *Phys. Rev. E 55*, 4617-4626 (1997).

Kleeorin, N.I. and Ruzmaikin, A.A., 'Mean-field dynamo with cubic non-linearity,' *Astron. Nachr. 305*, 265-275 (1984).

Krause, F. and Rädler, K.-H., *Mean Field Magnetohydrodynamics and Dynamo Theory*, Akademie-Verlag, Berlin (1980).

Kuang, W. and Bloxham, J., 'An Earth-like numerical dynamo model,' *Nature 389*, 371-374 (1997).

Laske, G. and Masters, G., 'Limits on differential rotation of the inner core from an analysis of the Earth's free oscillations,' *Nature 402*, 66-69 (1999).

Le Mouël, J.-L., Allègre, C.J. and Narteau, C., 'Multiple scale dynamo,' *Proc. Natl. Acad. Sci. USA 94*, 5510-5514 (1997).

Levy, E.H., 'Kinematic reversal schemes for the geomagnetic dipole,' *Astrophys. J. 171*, 635-642 (1972).

Mazaud, A. and Laj, C., 'Simulation of geomagnetic polarity reversals by a model of interacting dipole sources,' *Earth Planet. Sci. Lett. 92*, 299-306 (1989).

McFadden, P.L. and Merrill, R.T., 'Fundamental transitions in the geodynamo as suggested by paleomagnetic data,' *Phys. Earth Planet. Inter. 91*, 253-260 (1995).

Meinel, R. and Brandenburg, A., 'Behaviour of highly supercritical α-effect dynamos,' *Astron. Astrophys. 238*, 369-376 (1990).

Merrill, R.T., McElhinny, M.W. and McFadden, P.L., *The Magnetic Field of the Earth*, Academic Press (1996).

Merzbacher, E., *Quantum Mechanics*, Wiley, New York (1970).

Moffatt, H.K., *Magnetic Field Generation in Electrically Conducting Fluids*, Cambridge University Press (1978).

Narteau, C., Blanter, E., Le Mouël, J.-L., Shirnman, M. and Allègre, C.J., 'Reversal sequence in a multiple scale dynamo mechanism,' *Phys. Earth Planet. Inter. 120*, 271-287 (2000).

Olson, P., 'Geomagnetic polarity reversals in a turbulent core,' *Phys. Earth Planet. Inter. 33*, 260-274 (1983).

Olson, P. and Hagee, V.L., 'Geomagnetic polarity reversals, transition field structure, and convection in the outer core,' *J. Geophys. Res. 95*, 4609-4620 (1990).

Olson, P., Christensen, U. and Glatzmaier, G.A., 'Numerical modeling of the geodynamo: Mechanisms of field generation and equilibration,' *J. Geophys. Res. 104*, 10383-10404 (1999).

Ossendrijver, A.J.H., *Fluctuations and energy balance in solar and stellar dynamos*, Ph.D. Thesis, University of Utrecht, 1996.

Ossendrijver, A.J.H., Hoyng, P. and Schmitt, D., 'Stochastic excitation and memory of the solar dynamo,' *Astron. Astrophys. 313*, 938-948 (1996).

Otmianowska-Mazur, K., Rüdiger, G., Elstner, D. and Arlt, R., 'The turbulent EMF as a time series and the 'quality' of dynamo cycles,' *Geophys. Astrophys. Fluid Dynamics 86*, 229-247 (1997).

Parker, E.N., 'The occasional reversal of the geomagnetic field,' *Astrophys. J. 158*, 815-827 (1969).

Richards, P.G., 'Earth's inner core – discoveries and conjectures,' *Astron. Geophys. 41*, 1.20-1.24 (2000).

Risken, H., *The Fokker-Planck Equation*, Springer-Verlag, Berlin (1984).

Roberts, P.H. and Soward, A.M., 'Dynamo theory,' *Ann. Rev. Fluid Mech. 24*, 459-512 (1992).

Rüdiger, G., 'Behandlung eines einfachen hydromagnetischen Dynamos mittels Linearisierung,' *Astron. Nachr. 294*, 183-186 (1973).

Sarson, G.R. and Jones, C.A., 'A convection driven geodynamo reversal model,' *Phys. Earth*

Planet. Inter. 111, 3-20 (1999).

Schmitt, D. and Schüssler, M., 'Non-linear dynamos,' *Astron. Astrophys. 223*, 343-351 (1989).

Schmitt, D., Ossendrijver, M.A.J.H. and Hoyng, P., 'A bistable dynamo model explaining the geomagnetic secular variation and reversal records,' *Phys. Earth Planet. Inter.*, submitted (2000).

Song, X. and Richards, P.G., 'Seismological evidence for differential rotation of the Earth's inner core,' *Nature 382*, 221-224 (1996).

Souriau, A., Roudil, P. and Moynot, B., 'Inner core differential rotation: facts and artefacts,' *Geophys. Res. Lett. 24*, 2103-2106 (1997).

Soward, A.M., 'The Earth's dynamo,' *Geophys. Astrophys. Fluid Dynamics 62*, 191-209 (1991).

Stix, M., 'The solar dynamo,' *Geophys. Astrophys. Fluid Dynamics 62*, 211-228 (1991).

Su, W., Dziewonski, A.M. and Jeanloz, R., 'Planet within a planet: rotation of the inner core of the Earth,' *Science 274*, 1883-1887 (1996).

Valet, J.-P. and Meynadier, L., 'Geomagnetic field intensity and reversals during the past four million years,' *Nature 366*, 234-238 (1993).

Van Kampen, N.G., 'Stochastic Differential Equations,' *Phys. Reports 24C*, 171-228 (1976).

Van Kampen, N.G., *Stochastic Processes in Physics and Chemistry*, North-Holland, Amsterdam (1992).

Vidale, J.E., Dodge, D.A. and Earle, S.E., 'Slow differential rotation of the Earth's inner core indicated by temporal changes in scattering,' *Nature 405*, 445-448 (2000).

A Derivation of the Fokker-Planck equation

A.1 Notation

The first step is to rewrite Eq. (29) in terms of real numbers only. This is just a matter of book-keeping. Consider a complex equation of the type ($\dot{} = \mathrm{d}/\mathrm{d}\tau$):

$$\dot{a}_i = B_{ik} a_k \ . \tag{A.1}$$

Its real and imaginary parts may be grouped together in a real supervector $\mathbf{a}$ and a real supermatrix $\mathbf{B}$ with twice as many components:

$$\mathbf{B} \ = \left(\begin{array}{c|c} \Re B & -\Im B \\ \hline \Im B & \Re B \end{array}\right) \ ; \qquad \mathbf{a} \ = \left(\begin{array}{c} \Re a_0 \\ \Re a_1 \\ \vdots \\ \Im a_0 \\ \Im a_1 \\ \vdots \end{array}\right) \tag{A.2}$$

Eq. (A.1) can now be written in terms of real numbers only:

$$\dot{\mathbf{a}}_\mu = \mathbf{B}_{\mu\nu} \mathbf{a}_\nu \ , \tag{A.3}$$

Supervectors with 2∞ elements and $2\infty \times 2\infty$ supermatrices are indicated by boldface symbols, and as a further distinction Greek indices are employed. The mode equations (29) now read

$$\dot{\mathbf{a}}_\mu \ = \ \Big[\mathbf{L}_{\mu\nu} \ + \ (1 - \mathbf{a}_0^2)\, \mathbf{E}_{\mu\nu} \ + \ \mathbf{V}_{\mu\nu}\Big] \ \mathbf{a}_\nu \ , \tag{A.4}$$

where $\mathbf{a}_\mu$, $\mathbf{E}_{\mu\nu}$ and $\mathbf{V}_{\mu\nu}$ are the 'superpartners' of a_i, E_{ik} and V_{ik} in (29), and

$$\mathbf{L} \;=\; \left(\begin{array}{ccc|ccc} \Re\lambda^0 & 0 & \cdots & -\Im\lambda^0 & 0 & \cdots \\ 0 & \Re\lambda^1 & & 0 & -\Im\lambda^1 & \\ \vdots & & \cdot & \vdots & & \cdot \\ \hline \Im\lambda^0 & 0 & \cdots & \Re\lambda^0 & 0 & \cdots \\ 0 & \Im\lambda^1 & & 0 & \Re\lambda^1 & \\ \vdots & & \cdot & \vdots & & \cdot \end{array}\right) \;, \tag{A.5}$$

with $\Re\lambda^0 = \Im\lambda^0 = 0$.

A.2 Probability distribution of $\{\mathbf{a}_\nu\}$

The second step is to derive the joint probability distribution $\Pi(\mathbf{a},\tau)$ of $\{\mathbf{a}_\nu\}$. Eq. (A.4) defines an orbit in **a**-space (Figure 6) Consider many copy systems (A.4) each with a different realisation $\delta\alpha$. The density $f(\mathbf{a},\tau)$ of these systems obeys the continuity equation in **a**-space:

$$\frac{\partial f}{\partial \tau} \;=\; -\frac{\partial}{\partial \mathbf{a}_\mu}\,\dot{\mathbf{a}}_\mu f \;=\; [\mathcal{A}+\mathcal{V}(t)]\,f \;, \tag{A.6}$$

The operators $\mathcal{A}$ and $\mathcal{V}$ are defined as

$$\mathcal{A} \;=\; -\frac{\partial}{\partial \mathbf{a}_\mu}\left[\mathbf{L}_{\mu\nu} \;+\; s(1-\mathbf{a}_0^2)\,\mathbf{E}_{\mu\nu}\right]\mathbf{a}_\nu \;, \tag{A.7}$$

$$\mathcal{V} \;=\; -\frac{\partial}{\partial \mathbf{a}_\mu}\,\mathbf{V}_{\mu\nu}\mathbf{a}_\nu \;. \tag{A.8}$$

Eq. (A.6) is a stochastic differential equation for f with a multiplicative noise term $\mathcal{V}$. To get the probability distribution $\Pi(\mathbf{a},\tau) \equiv \langle f\rangle$, an average must be performed over the fluctuations. According to standard theory (Van Kampen, 1976, 1992):

$$\frac{\partial \Pi}{\partial \tau} \;=\; \left[\mathcal{A} \;+\; \int_0^\infty \mathrm{d}s\,\langle \mathcal{V}(\tau)\,\exp(s\mathcal{A})\,\mathcal{V}(\tau-s)\rangle\,\exp(-s\mathcal{A})\right]\Pi \;, \tag{A.9}$$

provided the correlation time τ_c is sufficiently small:

$$|\mathcal{V}|\tau_\mathrm{c} \ll 1 \;, \tag{A.10}$$

where $|\mathcal{V}|$ is the order of magnitude of $\mathcal{V}$. The validity of (A.10) is verified in Appendix C. The exponential operators can be elaborated with the help of Lagrangian co-ordinates (Van Kampen, 1992), but this is rather complicated. Since $\langle \mathcal{V}(\tau)\mathcal{V}(\tau-s)\rangle$ vanishes for $|s| \gtrsim \tau_\mathrm{c}$, we make the approximation $\exp(\pm s\mathcal{A}) \simeq 1$ ('no appreciable evolution during a correlation time τ_c'). This seems reasonable for the lower order eigenmodes in $\mathcal{A}$ with their long time scales. But the higher order modes with shorter time scales are also present, and hence there are time scales in $\mathcal{A}$ compared to which τ_c is not small. We are thus effectively assuming that high-order modes contribute little. Inserting the operators $\mathcal{A}$ and $\mathcal{V}$ in (A.9) we obtain:

$$\frac{\partial \Pi}{\partial \tau} \;=\; -\frac{\partial}{\partial \mathbf{a}_\mu}\left(\mathbf{N}_{\mu\nu}\mathbf{a}_\nu \;-\; \mathbf{M}_{\mu\nu\rho\sigma}\mathbf{a}_\nu\,\frac{\partial}{\partial \mathbf{a}_\rho}\,\mathbf{a}_\sigma\right)\Pi \;, \tag{A.11}$$

with

$$\mathbf{N} \;=\; \mathbf{L} \,+\, s(1-\mathbf{a}_0^2)\,\mathbf{E}\;, \tag{A.12}$$

$$\mathbf{M}_{\mu\nu\rho\sigma} \;=\; \int_0^\infty \mathrm{d}s\,\langle \mathbf{V}_{\mu\nu}(\tau)\mathbf{V}_{\rho\sigma}(\tau-s)\rangle\;. \tag{A.13}$$

The fluctuations are taken to be stationary so that $\mathbf{M}$ does not depend on τ. The operator identity

$$\mathbf{a}_\nu \frac{\partial}{\partial \mathbf{a}_\rho} \;=\; \frac{\partial}{\partial \mathbf{a}_\rho}\mathbf{a}_\nu \;-\; \delta_{\nu\rho}\;, \tag{A.14}$$

is inserted, together with the fact that $\mathbf{M}_{\mu\nu\nu\sigma} = 0$. This identity is a consequence of the specific form of V in (27) and the completeness of the eigenfunctions, see Appendix D. Then we find a Fokker-Planck equation for Π:

$$\frac{\partial \Pi}{\partial \tau} \;=\; -\frac{\partial}{\partial \mathbf{a}_\mu}\left(\mathbf{N}_{\mu\nu}\mathbf{a}_\nu \;-\; \mathbf{M}_{\mu\nu\rho\sigma}\frac{\partial}{\partial \mathbf{a}_\rho}\mathbf{a}_\nu\mathbf{a}_\sigma\right)\Pi\;. \tag{A.15}$$

The matrix elements $\mathbf{M}_{\mu\nu\rho\sigma}$ are constants, but $\mathbf{N}_{\mu\nu}$ is a function of $\mathbf{a}_0$.

A.3 Probability distribution of $\mathbf{a}_0$

Since we are only interested in the behavior of the fundamental mode, the third step is to eliminate the higher modes by integrating (A.15) over all $\mathbf{a}_\kappa$, except $\mathbf{a}_0$. The probability distribution of $\mathbf{a}_0$ is defined as

$$p(\mathbf{a}_0,\tau) \;=\; \prod_{\bar\kappa}\int \mathrm{d}\mathbf{a}_{\bar\kappa}\;\Pi\;. \tag{A.16}$$

The bar on κ indicates that the value $\kappa = 0$ is excluded. We integrate Eq. (A.15) as in (A.16), using (1) that terms of the type $\partial(\cdots)/\partial\mathbf{a}_{\bar\mu}$ vanish since they can be integrated and $\Pi \to 0$ when any $\mathbf{a}_{\bar\mu}$ approaches $\pm\infty$, and (2) that $\prod_{\bar\kappa}\int \mathrm{d}\mathbf{a}_{\bar\kappa}$ commutes with $\mathbf{a}_0$ and hence with $\partial/\partial\mathbf{a}_0$ and the matrices $\mathbf{N}$ and $\mathbf{M}$. The integrations are straightforward and the result is Eq. (32). The drift coefficient S and diffusion coefficient D are given by

$$S \;=\; \mathbf{N}_{00}\,a \,+\, \mathbf{N}_{0\bar\nu}\,\langle \mathbf{a}_{\bar\nu}\rangle|_a\;, \tag{A.17}$$

$$\begin{aligned} D \;=\; 2\Big(&\mathbf{M}_{0000}\,a^2 \,+\, \mathbf{M}_{0\bar\nu 0\bar\sigma}\,\langle \mathbf{a}_{\bar\nu}\mathbf{a}_{\bar\sigma}\rangle|_a \\ &+\, \mathbf{M}_{000\bar\sigma}\,a\,\langle \mathbf{a}_{\bar\sigma}\rangle|_a \,+\, \mathbf{M}_{0\bar\nu 00}\,a\,\langle \mathbf{a}_{\bar\nu}\rangle|_a\Big)\;. \end{aligned} \tag{A.18}$$

The overbars indicate that the fundamental mode 0 is excluded from the summation, and we have reverted to the simpler notation $a \equiv \mathbf{a}_0$. The conditional averages are to be evaluated at a fixed value of a:

$$\langle \mathbf{a}_{\bar\nu}\mathbf{a}_{\bar\sigma}\rangle|_a \;=\; \frac{\prod_{\bar\kappa}\int \mathrm{d}\mathbf{a}_{\bar\kappa}\;\mathbf{a}_{\bar\nu}\mathbf{a}_{\bar\sigma}\,\Pi}{\prod_{\bar\kappa}\int \mathrm{d}\mathbf{a}_{\bar\kappa}\;\Pi}\;, \tag{A.19}$$

and similarly for $\langle \mathbf{a}_{\bar\nu}\rangle|_a$. In principle, these averages may be computed from the stationary solution Π of Eq. (A.15), or by taking appropriate moments of that equation. This would in turn permit evaluation of (A.19), and hence of (A.17) and (A.18), but we have not obtained any useful results.

B Drift and diffusion coefficients

B.1 Drift coefficient

The first part of (33) follows from (A.17) and $\mathbf{N}_{00} = \mathbf{L}_{00} + s(1-\mathbf{a}_0^2)\,\mathbf{E}_{00} = \mu(1-a^2)$, since $\lambda^0 = 0$; $\mu = s\mathbf{E}_{00}$. Then we compute

$$\begin{aligned}
\mathbf{N}_{0\bar{\nu}}\,\mathbf{a}_{\bar{\nu}} &= [\mathbf{L}_{0\bar{\nu}} + s(1-\mathbf{a}_0^2)\,\mathbf{E}_{0\bar{\nu}}]\,\mathbf{a}_{\bar{\nu}} \\
&= s(1-\mathbf{a}_0^2)\,\Big(\Re E_{01}\,\Re a_1 + \Re E_{02}\,\Re a_2 + \cdots \\
&\qquad\qquad - \Im E_{00}\,\Im a_0 - \Im E_{01}\,\Im a_1 - \cdots\Big) \\
&= s(1-\mathbf{a}_0^2)\,\Re\sum_{k\geq 1} E_{0k}a_k\ , \qquad\qquad \text{(B.1)}
\end{aligned}$$

because $\mathbf{L}_{0\bar{\nu}} = 0$ (due to $\Im\lambda^0 = 0$), and $\Im E_{00} = 0$. To get $g_1(a) = \mathbf{N}_{0\bar{\nu}}\,\langle\mathbf{a}_{\bar{\nu}}\rangle|_a$, we insert (B.1) and then (30), and define

$$T_+ \equiv \Re\sum_{k\geq 1} a_k T_k \;=\; \Re(T - a_0 T_0)\ , \qquad \text{(B.2)}$$

which is the physical toroidal field minus the contribution of the fundamental mode. Finally the averaging is applied, and we obtain:

$$g_1(a) \;=\; s(1-a^2)\int_0^\pi \mathrm{d}\theta\,\sin\theta\cos\theta\,\tilde{P}_0\,\langle T_+\rangle|_a\ . \qquad \text{(B.3)}$$

On symmetry grounds, $\langle T_+\rangle|_a$ is zero for $a = 0$, so that $\langle T_+\rangle|_a \propto a$ for small a. This leads to a series expansion of the type $g_1(a)/(1-a^2) = Aa(1 + Ba^2 + \cdots)$. For our purposes the lowest order approximation $g_1(a) = A(1-a^2)a$ is sufficient. In that case the drift coefficient S as a whole will behave as $S = \text{const}\cdot(1-a^2)a$. Since S describes the systematic evolution of a, the constant must be equal to the exponential growth rate λ^0 at $C = C_\mathrm{m}$, which proves expression (33) for small a. Numerical experiments have confirmed (33) to be accurate for $|a| \lesssim 0.4$ (Section 5.1).

B.2 Diffusion coefficient

We begin with $D_0 = 2\mathbf{M}_{0000}$. According to (A.13):

$$\begin{aligned}
\mathbf{M}_{0000} &= \int_0^\infty \mathrm{d}s\,\langle\mathbf{V}_{00}(\tau)\mathbf{V}_{00}(\tau-s)\rangle \\
&= \int_0^\infty \mathrm{d}s\,\langle V_{00}(\tau)V_{00}(\tau-s)\rangle\ , \qquad\qquad \text{(B.4)}
\end{aligned}$$

since V_{00} is real. Insert (31):

$$\begin{aligned}
\mathbf{M}_{0000} &= \int_0^\infty \mathrm{d}s\int_0^\pi\int_0^\pi \mathrm{d}\theta\mathrm{d}\psi\,\sin\theta\sin\psi \\
&\qquad \times \tilde{P}_0(\theta)T_0(\theta)\tilde{P}_0(\psi)T_0(\psi)\left\langle\frac{\delta\alpha(\theta,\tau)}{\alpha_0}\,\frac{\delta\alpha(\psi,\tau-s)}{\alpha_0}\right\rangle\ . \qquad \text{(B.5)}
\end{aligned}$$

The autocorrelation function of $\delta\alpha(\theta,\tau)/\alpha_0 = fF(\theta,\tau)/\sqrt{2N_c \sin\theta}$ follows from that of F. According to the definition of F in Section 2.2.3:

$$\left\langle \frac{\delta\alpha(\theta,\tau)}{\alpha_0}\,\frac{\delta\alpha(\theta-\zeta,\tau-\sigma)}{\alpha_0}\right\rangle = \frac{f^2\,\langle F(\theta,\tau)F(\theta-\zeta,\tau-\sigma)\rangle}{2N_c\sqrt{\sin\theta\sin(\theta-\zeta)}}$$

$$= \frac{f^2\,(1-|\zeta|/\theta_c)\,(1-|\sigma|/\tau_c)}{2N_c\sqrt{\sin\theta\sin(\theta-\zeta)}} \qquad \text{(B.6)}$$

$$\simeq \frac{f^2\tau_c\theta_c}{2N_c\sin\theta}\,\delta(\zeta)\,\delta(\sigma)\;. \qquad \text{(B.7)}$$

In (B.6) the correlation function is understood to be zero for $|\zeta| > \theta_c$ or $|\sigma| > \tau_c$. The last expression (B.7) is a good approximation when τ_c is much smaller than the relevant time scales and $\theta_c = \pi/N_c$ is much smaller that the relevant spatial scales. This applies here as we are dealing with the fundamental mode which has a large-scale structure. It follows that $\mathbf{M}_{0000}$ is equal to

$$\mathbf{M}_{0000} = \frac{\pi f^2\tau_c}{2N_c^2}\int_0^\infty \mathrm{d}s\,\delta(s)\int_0^\pi\int_0^\pi \mathrm{d}\theta\mathrm{d}\psi\,\sin\psi$$

$$\times\,\tilde{P}_0(\theta)T_0(\theta)\tilde{P}_0(\psi)T_0(\psi)\,\delta(\theta-\psi)\;, \qquad \text{(B.8)}$$

which leads directly to (36), since $\int_0^\infty \delta(s)\,\mathrm{d}s = \frac{1}{2}$ and $D_0 = 2\mathbf{M}_{0000}$. Next in line is

$$\mathbf{M}_{0\bar{\nu}0\bar{\sigma}}\,\langle \mathbf{a}_{\bar{\nu}}\mathbf{a}_{\bar{\sigma}}\rangle|_a = \int_0^\infty \mathrm{d}s\,\langle \mathbf{V}_{0\bar{\nu}}(\tau)\mathbf{V}_{0\bar{\sigma}}(\tau-s)\rangle\,\langle \mathbf{a}_{\bar{\nu}}\mathbf{a}_{\bar{\sigma}}\rangle|_a\;. \qquad \text{(B.9)}$$

First, $\mathbf{V}_{0\bar{\nu}}\,\mathbf{a}_{\bar{\nu}}$ is evaluated with the help of (A.2):

$$\mathbf{V}_{0\bar{\nu}}\,\mathbf{a}_{\bar{\nu}} = \Re V_{01}\,\Re a_1 + \Re V_{02}\,\Re a_2 + \cdots$$

$$- \Im V_{00}\,\Im a_0 - \Im V_{01}\,\Im a_1 - \cdots$$

$$= \Re\sum_{k\geq 1} V_{0k}a_k\;, \qquad \text{(B.10)}$$

since $\Im V_{00} = 0$. Insert (31) and use (B.2):

$$\mathbf{V}_{0\bar{\nu}}(\tau)\,\mathbf{a}_{\bar{\nu}} = \int_0^\pi \mathrm{d}\theta\,\sin\theta\,\tilde{P}_0\,T_+\,\frac{\delta\alpha(\theta,\tau)}{\alpha_0}\;. \qquad \text{(B.11)}$$

Substitution in (B.9) and replacing the averaging brackets at the right places, and use of (B.7) yields:

$$\mathbf{M}_{0\bar{\nu}0\bar{\sigma}}\,\langle \mathbf{a}_{\bar{\nu}}\mathbf{a}_{\bar{\sigma}}\rangle|_a = \frac{\pi f^2\tau_c}{2N_c^2}\int_0^\infty \mathrm{d}s\,\delta(s)\int_0^\pi\int_0^\pi \mathrm{d}\theta\mathrm{d}\psi\,\sin\psi$$

$$\times\,\tilde{P}_0(\theta)\tilde{P}_0(\psi)\,\langle T_+(\theta)T_+(\psi)\rangle|_a\,\delta(\theta-\psi)\;, \qquad \text{(B.12)}$$

which leads to (37), allowing for a factor 2. Relation (B.12) assumes that the low order modes are the dominant contributors to T_+, so that the assumption of a δ-peaked correlation function in θ is justified.

The last contribution to D is $g_2(a) = 2a(\mathbf{M}_{000\bar{\sigma}}\langle \mathbf{a}_{\bar{\sigma}}\rangle|_a + \mathbf{M}_{0\bar{\nu}00}\,\langle \mathbf{a}_{\bar{\nu}}\rangle|_a)$, the evaluation of which has no novel surprises. It turns out that both terms are equal, and the computation is quite analogous to those above:

$$g_2(a) = 2a\,\frac{\pi f^2\tau_c}{2N_c^2}\int_0^\pi \mathrm{d}\theta\,\sin\theta\,\tilde{P}_0^2T_0\,\langle T_+\rangle|_a\;. \qquad \text{(B.13)}$$

Numerical experiments have shown that $g_2(a)$ is always small with respect to D as given by (35), and therefore $g_2(a)$ is not mentioned in the main text.

C Short correlation time

To be able to verify condition (A.10), the order of magnitude $|\mathcal{V}|$ of $\mathcal{V}$ is needed. According to (A.8), $\mathcal{V} \sim \mathbf{V}_{\mu\nu}$, so that we may estimate $|\mathcal{V}|$ as the r.m.s. of a typical matrix element V_{ik}:

$$|\mathcal{V}|^2 \sim \langle |V_{ik}|^2 \rangle = \int_0^\pi \int_0^\pi \mathrm{d}\theta \mathrm{d}\psi \, \sin\theta \sin\psi \, (\tilde{P}_i^* T_k)_\theta (\tilde{P}_i^* T_k)_\psi^* \times \left\langle \frac{\delta\alpha(\theta,\tau)}{\alpha_0} \frac{\delta\alpha(\psi,\tau)}{\alpha_0} \right\rangle . \tag{C.1}$$

(no summation over i, k.) Inspection of (B.6) and (B.7), shows that the appropriate value of the correlation function in (C.1) is $(f^2/2N_\mathrm{c} \sin\theta)\theta_\mathrm{c}\delta(\theta-\psi)$, and it follows that:

$$|\mathcal{V}|^2 \sim \frac{\pi f^2}{2N_\mathrm{c}^2} \int_0^\pi \mathrm{d}\theta \, \sin\theta \, |\tilde{P}_i^* T_k|^2 . \tag{C.2}$$

The eigenfunctions become more structured for increasing k, i, resulting in destructive interference, and we expect that the integral will be largest for $i = k = 0$, in which case (C.2) equals D_0/τ_c. Accordingly, an appropriate condition for the correlation time to be short is:

$$|\mathcal{V}|\tau_\mathrm{c} \sim (D_0\tau_\mathrm{c})^{1/2} \ll 1 . \tag{C.3}$$

This appears to be satisfied, since for our standard run $\pi f^2 \tau_\mathrm{c}^2 / 2N_\mathrm{c}^2 \simeq 1.6 \times 10^{-3}$, and the integral in (36) equals 3.529, so that $(D_0\tau_\mathrm{c})^{1/2} \simeq 7.5 \times 10^{-2}$.

D Proof of $\mathbf{M}_{\mu\nu\nu\sigma} = 0$

We infer from (A.13) that $\mathbf{M}_{\mu\nu\nu\sigma} = \int_0^\infty \mathrm{d}s \, \langle \mathbf{V}(\tau) \cdot \mathbf{V}(\tau - s) \rangle_{\mu\sigma}$, and by using the definition (A.2) for $\mathbf{V}$ we obtain, writing time arguments temporarily as upper indices:

$$\mathbf{V}^\tau \cdot \mathbf{V}^{\tau-s} = \left(\begin{array}{c|c} \Re\{V^\tau \cdot V^{\tau-s}\} & -\Im\{V^\tau \cdot V^{\tau-s}\} \\ \hline \Im\{V^\tau \cdot V^{\tau-s}\} & \Re\{V^\tau \cdot V^{\tau-s}\} \end{array} \right) , \tag{D.1}$$

where V^τ is the matrix defined in (31). We shall show that $V^\tau \cdot V^{\tau-s} = 0$, using the efficient bra and ket notation $\boldsymbol{b} = |b)$, $\tilde{\boldsymbol{b}} = (b|$ from quantum mechanics (Merzbacher, 1970). Specifically for eigenfunctions $\boldsymbol{b}_i = |i)$, $\tilde{\boldsymbol{b}}_j = (j|$. The inner product (13) is written as $(b_1|b_2)$, while (12) now reads $(i|j) = \delta_{ij}$. The expansion (14) may be written as $|b) = (k|b)|k) = |k)(k|b)$. Since this must hold for any $|b)$ it follows that $|k)(k| = 1$ (summation convention), the unit operator in function space. Explicitly:

$$\{|k)(k|\}_{nm} = \delta_{nm}\delta(\theta-\psi) . \tag{D.2}$$

n, m enumerate the poloidal and toroidal components of $|k)(k|$ as a 2×2 matrix, and the continuous indices θ, ψ are the arguments of $|k)$ and $(k|$, respectively. Relation (D.2) is a consequence of the supposed completeness of the eigenfunctions and is known as the completeness relation (Merzbacher, 1970). For example, the $n, m = 1, 2$ element of (D.2) reads explicitly: $\sum_k \tilde{T}_k^*(\psi) P_k(\theta) = 0$.

After these preliminaries the proof is simple. Since V given by (27) obeys $V(1)V(2) = 0$, where 1 and 2 stand for two different sets of arguments θ, τ of $\delta\alpha$, all matrix elements must also vanish. With (D.2) we get:

$$0 \;=\; (i|V(1)V(2)|j) \;=\; (i|V(1)|k)(k|V(2)|j) \;=\; V_{ik}(\tau_1)V_{kj}(\tau_2)\;, \tag{D.3}$$

where V_{ik} is the matrix element (31). In the notation of relation (D.1) it follows that $V^{\tau_1} \cdot V^{\tau_2} = 0$. The bottom line is that since $V(1)V(2) = 0$ in the representation of (27), it is zero in any equivalent representation.

E The scaling of c^2 and γ

The parameters c^2 and γ are defined as combinations of the constants Λ, Δ_0 and Δ_1 that occur in the drift coefficient S and diffusion coefficient D, and these are in turn fixed by the dynamo model. The Fokker-Planck equation (32) and therefore c^2 and γ derive ultimately from (A.15). This equation depends on the model parameters kR and $C_{\rm m}$ and on the overall factor $f^2\tau_{\rm c}/N_{\rm c}^2$ in $\mathbf{M}$, as may be gleaned e.g. from relation (B.8) for M_{0000}. This proves that c^2 and γ depend on the parameters f, $\tau_{\rm c}$ and $N_{\rm c}$ only through the combination $f^2\tau_{\rm c}/N_{\rm c}^2$, but the exact functional dependence remains unknown. The big challenge is to find the dependence of $\langle T_+^2\rangle|_{a=0}$ on $f^2\tau_{\rm c}/N_{\rm c}^2$. If we ignore this and take $\langle T_+^2\rangle|_{a=0}$ constant, we get, for fixed kR and $C_{\rm m}$:

$$\gamma \;\sim\; \left(\frac{f^2\tau_{\rm c}}{N_{\rm c}^2}\right)^{-1}\;, \qquad c^2 \;\sim\; \text{constant} \tag{E.1}$$

which is not too bad as a first approximation, see Table 2.

The fact that c^2 and γ depend only on $\langle T_+^2\rangle$ near $a = 0$ is remarkable. It suggests that there should be a simpler way to arrive at Eq. (32) than through Appendices A and B, where $\boldsymbol{b}$ is first expanded in overtones, which then magically recombine into $\langle T_+^2\rangle$ upon integration. Accordingly, the Ansatz

$$\boldsymbol{b} = a\boldsymbol{b}_0 + \boldsymbol{b}_+ \tag{E.2}$$

is made, where $\boldsymbol{b}_+$ is the field of the overtones, and inserted in (26) which we write symbolically as $\dot{\boldsymbol{b}} = O\boldsymbol{b}$. The result is $\dot{a}\boldsymbol{b}_0 + \dot{\boldsymbol{b}}_+ = O\boldsymbol{b}_0 + O\boldsymbol{b}_+$. Taking the inner product with $\tilde{\boldsymbol{b}}_0$ we get $\dot{a} = (\tilde{\boldsymbol{b}}_0, O\boldsymbol{b}_0) + (\tilde{\boldsymbol{b}}_0, O\boldsymbol{b}_+)$, which is then used to eliminate $\dot{a}\boldsymbol{b}_0$ from the previous equation. The result is two coupled equations for a and $\boldsymbol{b}_+$ alone. These are not reproduced here because we have not been able to extract a credible derivation of Eq. (32) from them. But the fact that they exist proves that the statistical properties of the dipole mode will only depend on the collective effect of all overtones together.

F Evaluation of $\langle T_{\rm r}\rangle$

To evaluate the integrals in (57) write $p(a) = \exp[\psi(a)]$ as in (50) and $[D(y)p(y)]^{-1}$ $= \Delta_1^{-1}\exp[\phi(y)]$, with $\phi(y) = \gamma y^2 - \gamma(c^2+1)\ln(1 + y^2/c^2)$. Since $\phi(0) = \phi'(0) = 0$ and $\phi''(0) = -2\gamma/c^2 \equiv \phi_0''$ we may write:

$$\langle T_{\rm e}\rangle \;=\; \frac{2}{\Delta_1}\int_0^{a'} {\rm d}y\, \exp[\phi(y)] \int_y^{\infty} {\rm d}z\, \exp[\psi(z)] \tag{F.1}$$

$$\;\simeq\; \frac{2}{\Delta_1}\int_0^{\infty} {\rm d}y\, \exp(\tfrac{1}{2}\phi_0''\, y^2) \int_{-\infty}^{\infty} {\rm d}z\, \exp[\psi_{\rm m} + \tfrac{1}{2}\psi_{\rm m}''(z - a_{\rm m})^2] \tag{F.2}$$

$$\;=\; \frac{2\pi}{\Delta_1}\left(\frac{1}{\phi_0''\,\psi_{\rm m}''}\right)^{1/2} \exp(\psi_{\rm m}) \tag{F.3}$$

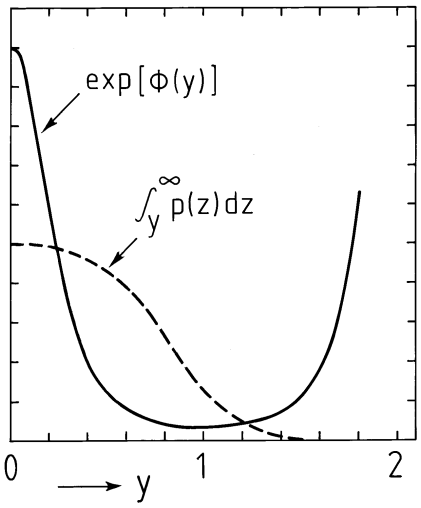

Figure 11: The functions $\exp[\phi(y)] = \Delta_1[D(y)p(y)]^{-1}$ and $\int_y^\infty p(z)\,\mathrm{d}z$ that occur in (57) and (F.1), for $\gamma = 3$ and $c^2 = 0.2$.

The approximation $\exp[\phi(y)] \simeq \exp(\frac{1}{2}\phi_0'' y^2)$ is adequate when the integration limit a' in (F.1) is about 1, see Figure 11. Subsequently, a' may be replaced by ∞ because $\exp(\frac{1}{2}\phi_0'' y^2) = \exp(-\gamma y^2/c^2) \to 0$. Likewise, the integration limit y in (F.1) may be replaced by zero because $\int_y^\infty p(z)\,\mathrm{d}z \approx \int_0^\infty p(z)\,\mathrm{d}z$ in the interval $[0, c/\sqrt{\gamma}\,]$ where $\exp[\phi(y)] = \exp(-\gamma y^2/c^2)$ contributes most, Figure 11, and after $\psi(z)$ has been expanded it may be replaced by $-\infty$. The remaining integrals in (F.2) are simple.

As the particle escapes from $[0, \infty]$ it is located at $a = 0$ and has two options: to fall in the well at $a = 1$, or in the well at $a = -1$. The probabilities for these two events would be equal if the subspace $a = a_0 = 0$ is the separatrix of the two basins of attraction. That is, when $a_0 = 0$, it should *remain* zero in the absence of fluctuations. But this is not the case since for $a_0 = 0$ and $V_{ik} = 0$, Eq. (29) says that $\mathrm{d}a_0/\mathrm{d}\tau = s\sum_{k\neq 0} E_{0k}a_k \neq 0$. It follows that there is a residual pulling on the dipole mode by the overtones that destroys the equal probability for escape to the left and to the right. Consequently, the relation $\langle T_\mathrm{r}\rangle = 2\langle T_\mathrm{e}\rangle$ is only approximate.

After substitution of ϕ_0'', of (54) and use of (44) we obtain (58). Subsequent substitution of (53) produces a complicated expression, whose asymptotic expansion is straightforward. The only nontrivial hurdle on the road to (59) is that

$$\left(\frac{\gamma c^2+\gamma-1}{\gamma c^2}\right)^{\gamma c^2+\gamma} = \left(\frac{1+c^2}{c^2}\right)^{\gamma(1+c^2)}\left(1-\frac{1}{\gamma(1+c^2)}\right)^{\gamma(1+c^2)}$$

$$\sim \left(\frac{1+c^2}{c^2}\right)^{\gamma(1+c^2)}\cdot \mathrm{e}^{-1}\,,$$

for γ large.